Crystal growth, structure and physical properties of crystals

[#]Novikov G.V., and Sipavina L.V. Clinopyroxenes and their Ge – analogs: strain tensor as a specific characteristic of the structure modification.

key words [*deformation clinopyroxene germanate*]

The unit cell deformation at isomorphic substitution or at temperature or pressure variation depends on elastic properties of crystal and, in principle, should be different for crystals with different kind of structure. The difference in elastic properties, even for close structures, could be fixed on distinctive character of the unit cell deformation at isomorphous substitution.

The strain ellipsoid provides a general description of the unit cell size and shape variation at isomorphic ion substitution, as well as at pressure and temperature changes. Strain tensor parameters behavior with the content, T or P could be used to distinguish close structural modifications of chain structures and to analyze the attendant variations in atomic bounding, and the difference in their elastic properties. Structural data on (Fe, Mg)-Ca and Fe-Mg monoclinic silicates and germanates with pyroxene structures were used to get the plots “unit cell parameter (a, b, c, β) – Volume V” and to evaluate the strain ellipsoid parameters for several distinct structural modifications, when composition, temperature or pressure (X-, T-, or P- trends) were variable, being the “trend-forming” parameters.

By the way of example, the X-trends (Figs.1,2) permit one to distinguish two close, but distinct monoclinic pyroxene structures, having the same space group C2/c, – the “C2/c-I” and the “C2/c-II” structural modifications. On the other hand, the specifically identical X-trends were found for monoclinic silicates and germanates, proving their crystal chemical identity.

At the first approximation, the character of deformation at the identical cation substitution along every crystal axis changes specifically, at the same time, it is distinctive for every structural pyroxene modification.

The numerical comparing of deformation characteristics of structures is also possible , as it was mentioned, for example, in [1]. More, relationship between lattice parameters and strain tensor components could be evaluated numerically and used with success. Results of such an analysis of strain tensor parameters for three structural modifications of monoclinic pyroxenes and their germanium analogs (Table I) have shown, that difference in elastic properties of “isostructural” pyroxenes with the space group C2/c manifests itself on X-trends distinctive enough. The results of the study show the applicability of strain tensor as a specific characteristic of the structural type for pyroxene structures.

[#] The work was supported by research grant N 98-05-64588 to Novikov G.V. from RFBR.

Table 1. Principal strain components due to chemical substitution for Mg-Fe and Ca-Fe monoclinic pyroxenes and related germanates.

	Principal strain components [x10^{-4} per 1% Fs or Wo]			Orientation of principal axes [angle, grad.]		
	ε(max)	ε(med)	ε(min)	**r_1**(max)	**r_2** (med)	**r_3** (min)
Di-Hd	2.2	1.4	-0.8	21.6	***b***	158.4
Ge-Di-Ge-Hd	2.7	0.62	-3.24	45	***b***	135
$MgSiO_3$-$FeSiO_3$(HP)	12.9	4.3	-2.7	18	***b***	172
$MgGeO_3$-$FeGeO_3$	8.5	2.3	-3.8	24	***b***	164
$^{1}Fs_{100}Wo_0$-$Fs_{85}Wo_{15}$	13	0.07	-.01	56	***b***	146
$^{1}Fs_{85}Wo_{15}$-$Fs_{75}Wo_{25}$	8.9	-1.7	-6.7	59	***b***	149
$^{1}Fs_{75}Wo_{25}$-$Fs_{65}Wo_{35}$	15	-2.5	-8.0	60	***b***	150
$^{1}Fs_{65}Wo_{35}$-$Fs_{50}Wo_{50}$	6	-0.5	-1.5	55	145	***b***
$Fg_{70}Wo_{30}$-$Fg_{60}Wo_{40}$	10.5	6.2	-2.6	4.1	175.9	***b***

Reference:

Y.Ohashi and C.W.Burnham (1973) Clinopyroxene lattice deformation: the roles of chemical substitution and temperature. // American Mineralogist, 58, 843-849

Mg →Fe, Fe ← Ca

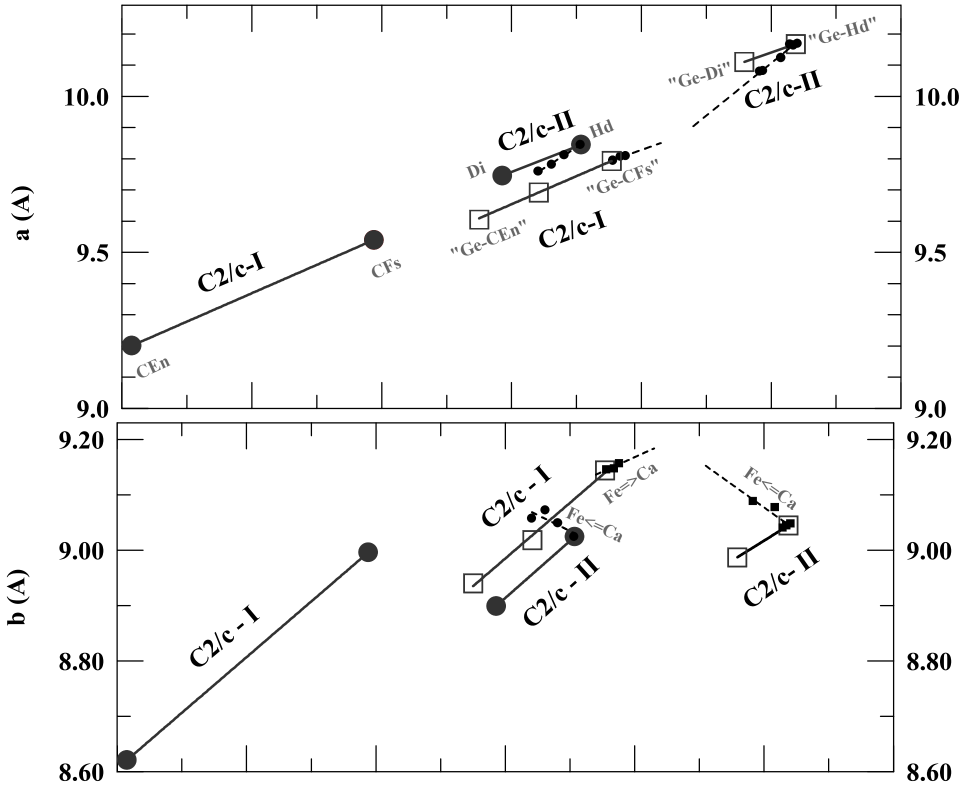

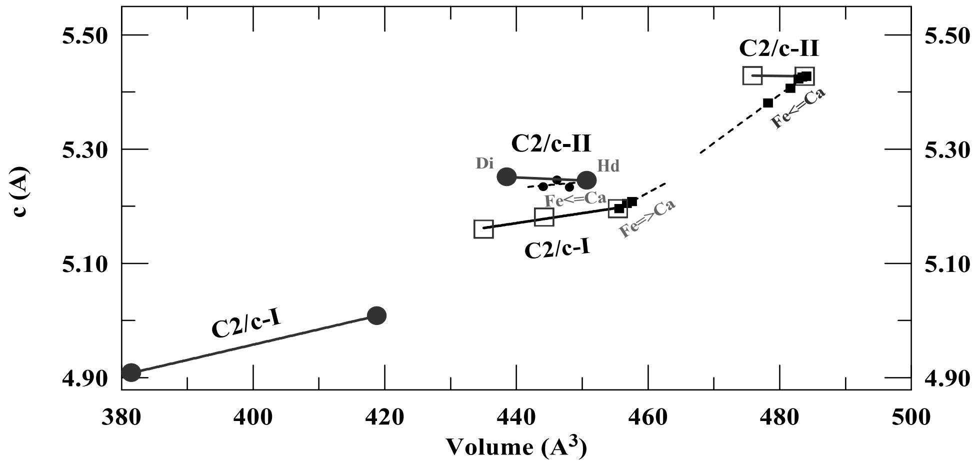

Fig. 1. The "Unit cell parameters (*a, b, c*) - Volume *V* " X-trends (Mg => Fe and Ca => Fe (small symbols)) for monoclinic germanates and silicates with pyroxene structure.

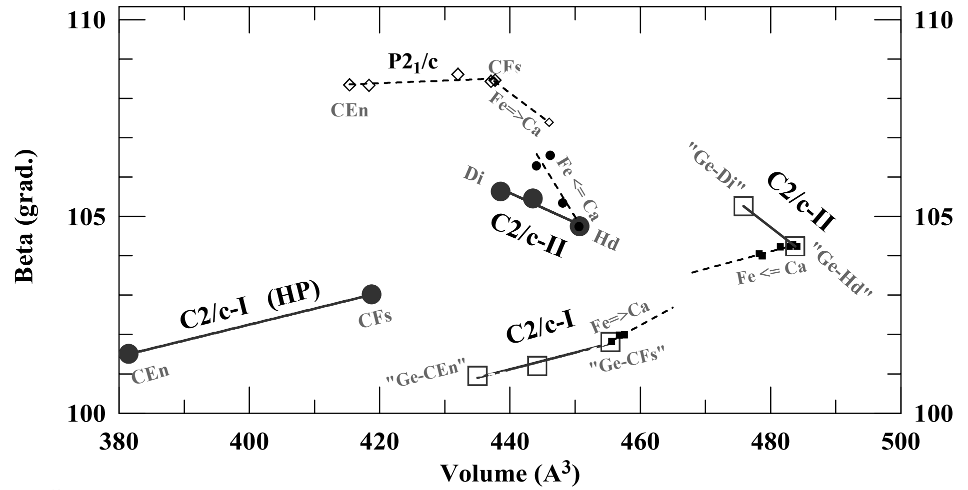

Fig. 2. The "*β* - *V* " X-trends (Mg => Fe and Ca => Fe (small symbols)) for monoclinic germanates and silicates with pyroxene structure. X-trends for the P2$_1$/c pyroxenes (rhombic symbols) are presented for comparison.

[#]Novikov G.V., and Sipavina L.V., Stuesser N., Hafner S.S. Phase transitions in germanates with pyroxene structure at low temperature.

key words [phase transition germanate]

Low temperature phase transitions in the Fe-Ca germanates ((Fe,Ca)GeO$_3$) with pyroxene structure, which are apparently analogous to transitions in orhoferrosilite, were studied by the nuclear gamma-resonance (NGR) spectroscopy, neutron diffraction and magnetic susceptibility methods. In particular, the orientation of the electric field gradient (EFG) tensor main axes relatively to crystal axes for two distinct magnetic phases in FeGeO3 was determined by NGR. The reorientation of magnetic moments in both the M1 and the M2 magnetic sublattices, accompanying one of the magnetic phase transitions, without change of crystal structure, was proved using low temperature neutron diffraction measurements. The inflection point on the magnetic susceptibility curve at T=12K supports the existence this phase transition just in the Ca-poor germanates.

The neutron scattering by magnetic moments below the Neel temperature (at T<T$_N$) due to the magnetic ordering in the system could be fixed by the appearance of reflexes of the first group. Analysis of relative intensities of these "magnetic reflexes" has shown, that magnetic moments are oriented along the crystallographic axes ***b*** at T<T$_N$. At very low temperature T<T$_M$, the new additional reflexes appear, proving, that the orientation of magnetic moments changes. The T$_M$ temperature appeared being close to the temperature, which was determined earlier by the NGR method [1].Taking into account the second group of "magnetic reflexes", we determined the orientation of magnetic moments being close to the crystal axes ***c*** .

It is to be mentioned, that at temperatures near to T$_M$ the moments change their orientation gradually in some temperature interval (Fig.2). The gradual increasing of all reflexes of this second group at T<T$_M$ correlates with the character of change of the ***θ*** angle between the iron magnetic moments and the EFG tensor main axis.

[#] The work was supported by research grant N 98-05-64588 to Novikov G.V. from RFBR

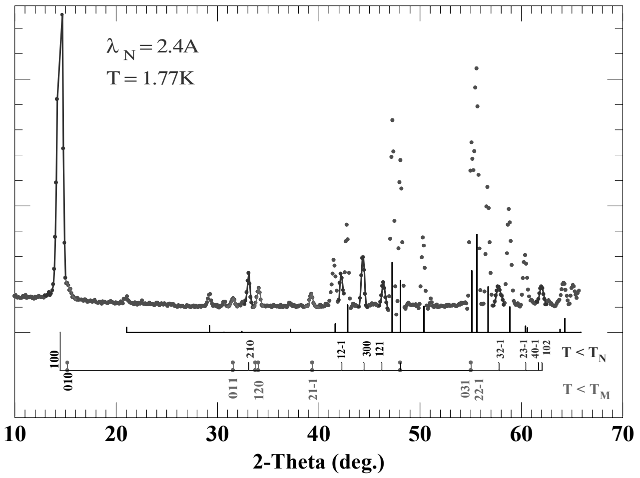

Fig 1. The neutron diffraction pattern of $FeGeO_3$ at T=1.77K. The "structural" reflexes are shown without reflection indices. Relative intensities are shown schematically for all reflections. Two groups of "magnetic" reflections with reflection indices, which appear just at magnetic ordering at T= T_N and at phase transition at T = T_M , are presented separately.

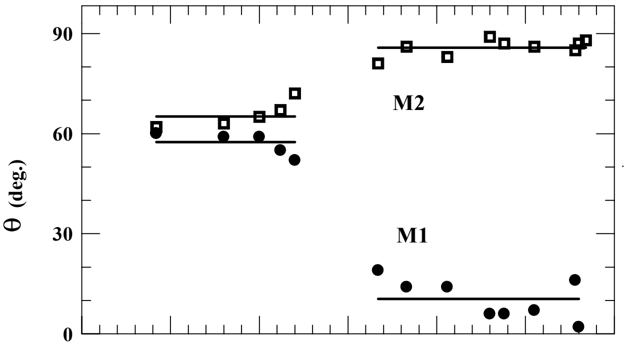

Fig.2.The temperature dependence of the θ angle between spins and EFG tensor main axis, and the relative intensities of the low temperature "magnetic reflexes" near to magnetic phase transition in germanate $FeGeO_3$ (space group C2/c).

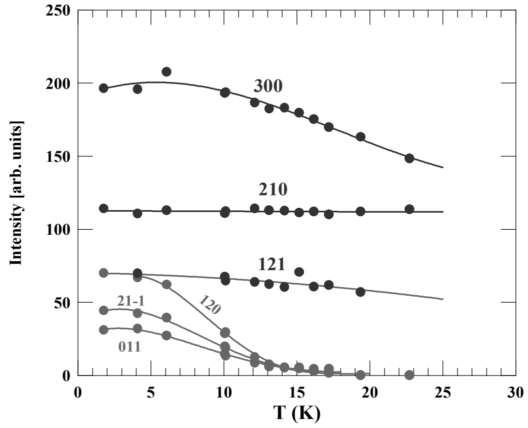

References:

1. G.V. Novikov, L.V. Sipavina and S.Hafner (1995) Low temperature magnetic transition in chain germanates. Solid State Commun., 95, 405-408.

[#]Suvorova V.A., Kotelnikov A.R. Investigation of synthetic Sr-bearing wollastonites (preliminary data)

key words: [*Sr-bearing wollastonite series, chemical and physical properties, unit-cell parameters*]

The purpose of this work is investigation of properties and determination of unit-cell parameters of synthesized solid solutions in $(Ca,Sr)SiO_3$ series with strontium mole fraction X_{Sr} = 0; 0.2; 0.4; 0.5; 0.6; 0.8 and 1.0. The synthesis of this wollastonite series, which is an intermediate component for titanite synthesis, was conducted during research on synthesis of Ca-Sr series of titanite as a potential concentrator of radioactive elements.

Stoichiometric mixtures of carbonate components and silicon dioxide were ground to homogeneous composition in ethanol in mechanic agate mortar, dried at 400°C during 4 hours and pressed as tablets by cold pressing. The obtained tablets were sintered at 1150°C during 24 hours then they were again ground, pressed as new tablets and sintered at 1180°C during 24 hours. The produced samples of ceramics had a density from 1.7 to 2.3 g/cm^3. Microprobe and x-ray investigations reveal a homogeneity of synthesized samples and correspondence of their stoichiometry in the series wollastonite – strontium analog of wollastonite. Chemical composition of synthesized wollastonites is presented in table 1.

[#] This work was financially supported by the Russian Foundation for Basic Research, project no. 97-05-65886.

Table 1. Oxide content (wt%) in wollastonites (microprobe data).

N of sample	SiO_2	CaO	SrO	Formula
W-II/0.0	59.76 (22*)	40.12(18)	-	$Ca_{0.972}Sr_{0.008}Si_{1.013}O_3$
W-II/0.2	49.82 (24)	36.74 (19)	13.37 (22)	$Ca_{0.804}Sr_{0.148}Si_{1.018}O_3$
W-II/0.4	46.06 (25)	23.90 (16)	30.01 (29)	$Ca_{0.574}Sr_{0.380}Si_{1.020}O_3$
W-II/0.5	42.49 (25)	21.05 (15)	36.41 (29)	$Ca_{0.528}Sr_{0.493}Si_{0.989}O_3$
W-II/0.6	43.79 (25)	15.47(13)	39.99 (29)	$Ca_{0.404}Sr_{0.544}Si_{1.025}O_3$
W-II/0.8	40.57 (25)	10.09(11)	49.31 (30)	$Ca_{0.242}Sr_{0.684}Si_{1.036}O_3$
W-II/1.0	38.67 (26)	-	61.19(31)	$Ca_{0.013}Sr_{0.942}Si_{1.027}O_3$

* - errors of composition identification (referred to the last tenth characters).

The unit-cell parameters were calculated for these solid solutions. The calculation was carried out in assumption of triclinic (pseudorhombic) structure. The results of calculations are presented in Table 2:

Table 2. Unit-cell parameters of (Ca,Sr)-wollastonites.

N	N of sample	X^{Sr}	a, (Å)	b, (Å)	c, (Å)	α, °	β, °	γ, °	V, (Å^3)	Ref.
1	W-II/0.0	0.0	6.845 (2*)	11.908 (2)	19.668 (2)	90.09 (2)	90.56 (2)	90.00 (2)	1603.9 (5)	1**
2	W-II/0.2	0.16	6.859 (1)	11.855 (3)	19.669 (4)	90.13 (2)	90.55 (1)	89.78 (1)	1599.1 (3)	1
3	W-II/0.4	0.40	6.855 (2)	11.863 (6)	19.701 (6)	90.09 (3)	90.52 (2)	89.78 (1)	1602.0 (6)	1
4	W-II/0.5	0.48	6.855 (1)	11.886 (2)	19.688 (2)	90.11 (1)	90.55 (1)	89.73 (1)	1604.1 (2)	1
5	W-II/0.6	0.57	6.876 (3)	11.873 (3)	19.664 (6)	89.99 (3)	90.40 (2)	89.72 (2)	1605.4 (5)	1
6	W-II/0.8	0.74	6.875 (2)	11.874 (1)	19.660 (4)	90.3 (1)	90.46 (1)	89.76 (1)	1604.9 (3)	1
7	W-II/1.0	1.0	6.876 (2)	1.863 (7)	19.655 (5)	89.93 (7)	90.40 (3)	89.74 (5)	1603.2 (7)	
8	Psevdo-wollast.	0.0	6.853 (3)	11.895 (5)	19.674 (13)	90.12 (3)	90.55 (3)	90.00 (3)	1603.7	2***

* - errors of unit-cell parameters determination (referred to the last tenth characters); ** - this paper; *** - Takamitsu, Y. and Hiroshi, M. (1981). Acta Cryst., B37, 1010-1017.

Conclusion

1. Solid solutions of (Ca,Sr)-wollastonites are synthesized at 1180°C. They are shown to form the series of continuous solid solutions at this temperature.

2. Unit-cell parameters are identified for synthetic samples.

Tikhomirova V.I., Chichagov A.V., Akhmedzhanova G.M. The regulated hydrothermal synthesis of geversite ($PtSb_2$)

key words *[synthesis geversite]*

Such minerals as sperrylite $PtAs_2$ and aurostibite $AuSb_2$ are found at the contacts of precious metal alloys in ultrabasic rocks, and resulted from high-temperature evolution of the magmatic process. Geversite is much more rare mineral. Therefore, the synthesis of these compounds from elements requires high temperatures, and, besides, conducting the process in closed furnaces in an inert environment, which prevents components, especially arsenic, from vaporization and oxidation.

On the other hand, the role of hydrothermal solutions, enriched in volatiles, increases at the formation of intermetalides of precious metals. The regulated crystallization under hydrothermal conditions requires information about base-acid and oxidation-reduction parameters, as well as concentrations of components in an experiment. Absence of sulfide components in solutions and reduced environments, preventing Sb from oxidation, is especially important for the regulated synthesis of $PtSb_2$.

Sperrylite [1] and aurostibite [2] were already synthesized in hydrothermal conditions, whereas geversite is known only as natural findings [3]. The study of stibium behavior under hydrothermal conditions has been carried out by some authors [4, 5]. They showed, that $Sb(OH)_3$ is the major stibium species in aqueous solutions.

The paper presents the detailed study of a mechanism of geversite synthesis. The method was described earlier in [2]. The conditions analogous to those of aurostibite synthesis from metallic components, placed in autoclaves of PH-8 alloy, in solutions of hydrochloric acid (0.001 -

0.500 N), rectified from oxygen by streaming argon. The solution occupied 0.75 of autoclave volume, which provided pressure of 500 bar at temperature 300^{O}C. The method of spectrophotometric analysis of stibium by coloration of its iodide complex was additionally worked out.

According to [4, 5], the predominant stibium species in the sulfide-free system at parameters of the experiment (300^{O}C and 500 bar) is $Sb(OH)_3$. Using regulation of pressure by hydrogen, the reaction of high-temperature stibium hydrolysis up to 450^{O}C:

$Sb + 3H_2O = Sb(OH)_3 + 1.5H_2$ (1)

was studied in detail [5], and equilibrium constant $K_1 = -1.09 \pm 0.12$ was obtained for 500 bar and 450^{O}C.

Using the same method of calculation, we obtained the equilibrium constant for reaction (1) $K_1 = +0.31$ for 500 bar and 300^{o}C and for $\lg fH_2 = +2.12$. Such constant shows, that the reaction is appreciably displaced towards dissolved stibium species. Such difference is apparently related to the presence of hydrochloric acid (from 0.001 to 0.1 mole) in our experiments. Therefore, transport of metallic stibium to solution can proceed by reaction

$Sb + 2HCl + H_2O = Sb(OH)Cl_2 + 1.5H_2$ (2).

It is supported by the dependence of stibium solubility on HCl concentration. Sb solubility in the 0.1 N HCl is $1.27 \cdot 10^{-3}$ mol/kg H_2O, whereas in the 0.5 N HCl it is $1.36 \cdot 10^{-2}$ mol/kg H_2O.

Having no thermodynamic data for $Sb(OH)Cl_2$ for calculation of the reaction, we used values of Gibbs free energies for the constituent ions from the SUPCRT-92 data base. Gibbs free energy for stibium oxychloride was calculated by combination of ΔG of $SbCl_2$ and OH^-, taken from [4]. The used values are listed in table 1. The obtained equilibrium constant for reaction (2) is $10^{-6.5}$, while equilibrium constant for reaction (1), calculated from the same data base, is 10^{-7}. It means, that at competition of reaction (1) and (2) in the presence of HCl the latter is predominant.

Table 1. Free energies of formation of compounds and species

	ΔG at 300°C and 500 bar		
Species	kJ/mol	kcal/mol	Reference
Sb	-14.178	-3.387	Robie, 1978
H_2 (gas)	-9.224	-2.204	Robie, 1995
OH^-	-142.616	-34.308	Robie , 1995
H_2O	-262.858	-62.824	Robie, 1995
$Sb(OH)_3$	-712.157	-170.128	Shik, 1988
$SbCl_{2-}$	-244.99 (1 kbar)	-58.526	Kolpakova, 1990
HCl^o	-98.81 (1 kbar)	-23.616	Kolpakova, 1990

Concentration of soluble stibium species decreases to $2.3 \cdot 10^{-4}$ mol/kg H_2O in the presence of metallic platinum in 0.1 N HCl solution, because of formation of some compounds.

Molecular hydrogen participates in the equilibria (1) and (2). Introduction of additional hydrogen can displace the equilibrium towards more oxidized or more reduced species.

In order to produce minerals with non-oxidized stibium we used the "in situ" experiments in which additional hydrogen was obtained through the interaction of metallic aluminum with water, that yields stoichiometric amount of hydrogen

$2Al + 4H_2O = 2\,AlOOH + 3H_2$ (3).

Hydrogen fugacity was calculated accounting for non-ideality of the H_2O+H_2 mixture [6], whereas hydrogen mole fraction was calculated from weight ratio of aluminum and water in an autoclave. At 300^{O}C and 500 bar for 100 mg of Al and degree of autoclave filling 75 % $\lg fH_2 = +2.12$.

Calculation of platinum potential as hydrogen electrode at 300^{O}C and given hydrogen fugacity shows value (-0.354 V) with respect to the hydrogen electrode. In acid aqueous-chloride solutions platinum solubility is conditioned by formation of chloride complexes of bi-valent platinum under hydrothermal conditions, especially at reducing buffers [7]. On the other hand, in the hydrogen presence the potential of metallic platinum can be identified with Eh value. If the latter is calculated accounting for all activity coefficient and dependence on hydrogen fugacity using the program by Shvarov [8], then $\lg fH_2 = +2.12$ for T = 573.15^{O}K (300^{O}C) and total pressure 500 bar.

Aqueous solution	Acid solution 0.1 N HCl
pH = 5.435	pH = 1.447
Eh = -0.739	Eh = -0.285

If, according to [7], in the experiments close to our (Ni/NiO buffer) at 300^{O}C platinum solubility was $5.7 \cdot 10^{-6}$ g/l, then at above potential equilibrium platinum concentration, as a potential of forming element, was 10^{-22} mol/kg of water. Thus, soluble platinum species in a solution have very low concentrations at such negative potentials.

Calculation was performed for reaction:

$Pt + 4Cl^- - 2e = PtCl_4^{-2}$(4).

In such conditions stibium is also reduced on the surface of the platinum electrode to form perfectly crystalline mineral, which was identified with x-ray analysis. The mineral belongs to the pyrite structural type, where the size of the "dumb-bell" bond Sb-Sb almost coincides with the size of the Pt-Sb bond, which provides an incredible stability of a cubic crystal [9].

References:

1. Evstigneeva T., Tarkian M. (1996) // European Journal of Mineralogy. . 8(3), p. 549-564.
2. Tikhomirova V.I. et al. (1998) // Experiment in Geosciences, V.7, N.2, p. 29-31.
3. Wyckoff R.W.Y. (1963) // Crystal structures, 1, 346-348.

4. Kolpakova N.N., Manucharyants B.O. (1990) // Geochimiya, , N 12, p. 1756-1768.
5. Shikina N.D., Zotov A.V. (1990) // Geochimiya, , N 12, p. 1767-1772.
6. Kishima N, sakai H. (1984) // Earth and Planet. Sci. Lett., V. 67, p. 79.
7. Pluysnina L.P., Nekrasov I. Ya., Shcheka Zh. A. (1995) // Doklady RAS, V. 340, p. 525-527.
8. Shvarov Yu.V. (1976) // Doklady RAS, V.5, p. 1224.
9. Chichagov A.V. et al. (1990) // Information-Calculating System on Crystal Structure Data of minerals (MINCRYST) // Kristallographia, , V.35, N3, p. 610-616.

[#]Stolyarova T.A. Thermodynamics of apatites

key words [*apatite whitlokite thermodynamic thermochemistry enthalphy*]

Theoretical compositions of apatites are characterised by high concentrations of volatile components, but natural isomorphous mixtures of apatites having such high concentrations of volatiles are of rare occurrence although their examples are cited in special mineralogic literature. A review of analyses of apatites reveals systematic deficiency of volatiles in the apatite compositions against their theoretical compositions. This feature of apatites has long drawn the researchers' attention and has been attributed to the incorporation into their composition of excessive oxygen which substitutes for fluorine, chlorine, and water with the formation of hypothetic end member - oxyapatite (voelckerite) $Ca_{10}P_6O_{25}$, its existence being, however, disputable [1]. Actually the incorporation of oxygen into the apatite composition in place of other volatiles necessitates highly oxidative conditions unattainable in natural mineral formation. It became especially clear when mineralogists began to study Moon's rocks and meteorites whose highly reductive formation conditions are attested by incorporation into their compositions of natural metals, these being not only iron and nickel, but silicon and aluminium as well. Nevertheless, the compositions of these cosmic objects and of the Earth's rocks do involve apatites depleted in volatile components. Apparently, this deficiency cannot be attributed to voelckerite, and some other phosphate component free of fluorine, chlorine, and water has to enter into the composition of isomorphous apatite series.

Mineralogic studies of meteorites and Moon's rocks have also added to the knowledge of diversity of minerals which enter into the apatite group when associations of this mineral with whitlokite and alkali magnesial phosphates, not normally found in Earth's rocks and apatite ores, were discovered. An example of such association is described [2]in an ordinary chondrite Yamato-82133, found in Antarctic, in its matrix enriched in nickel iron. Chlorapatite in this matrix enriched in nickel iron. Chlorapatite in this association differs from the theoretical composition ($Ca_5P_3O_{12}Cl$) in chlorine deficiency and admixture of MgO+FeO. In these features its composition is somewhat displaced towards the whitlokite composition although the MgO/FeO ratio in it is much lower than in whitlokite and alkali phosphate which are in association with it. This ratio decreases sequentially in the series chlorapatite - whitlokite-alkali phosphate. Nevertheless, the given ratios of the minerals composition are suggestive of isomorphous incorporation into the chlorapatite composition of a chlorine-free endmember close, to some extent, to whitlokite. Then the formula of apatite can be given as nAp(1-n)W, according to the analysis of [2]: $0.875(Ca_5P_3O_{12}Cl)\cdot 0.125(Na_{0.32}Ca_{4.24}Fe_{2.4}P_{2.56}O_{12})$.

Such an approach explains the usual deficiency of chlorine in the composition of natural chlorapatites the concentration of whichnever reaches 6.8 wt%, i.e. the value conforming to the theoretical formula. The water component is absent in apatites of extraterrestrial rocks which is attributed to deficiency of a water phase at their formation. The same accounts for the presence in meteorites of alkali phosphates that are readily soluble in water and do not form in the presence of water fluids inherent in terrestrial petrogenesis.

A study of fluoroapatites, containing very small amounts of chlorine and water, typical of alkali nepheline-syenite intrusions of the Kola peninsula (Khibinsky, Lovozersky and others) reveals a great deficiency of fluorine against the theoretical composition of fluorapatite (3.8 wt% F). Nearly complete isomorphism of fluoroapatite with calcium phosphate free of volatiles (compositionally close to whitlokite) is established.

Thermodynamic studies of this isomorphous series were carried out for apatite samples with a variable concentration of fluorine (table 1).

[#] The work was sponsored by the RFBR (Project N 97-05-64159)

Table 1. Compositions (wt%) of apatites, studied thermochemically

Components	1	2	3	4	5	6	7	8	9
SiO_2	0.70	0.46	-	0.21	0.64	0.43	0.44	1.02	1 .01
Al_2O_3	-	0.02	0.02	0.02	0.01	0.02	0.08	-	0.03
Fe_2O_3	-	0.22	0.53	0.04	0.61	0.45	0.13	0.05	0.06
La_2O_3	-	-	-	0.35	-	-	-	-	-
Y_2O_3	-	-	-	0.04	0.15	-	0.05	0.12	0.17
MgO	-	0.05	0.01	-	-	0.02	0.15	0.09	0.06
MnO	-	0.03	-	-	-	-	0.05	0.02	0.02
GaO	56.20	55.09	54.72	53.46	56.06	55.22	52.66	53.43	54.64
SrO	-	0.13	1.13	3.15	-	-	3.78	3.73	2.13
K_2O	0.04	-	0.06	0.11	0.09	0.06	0.13	-	-
Na_2O	-	-	0.28	0.13	0.17	0.41	0.22	-	-
P_2O_5	40.00	40.35	41.63	39.72	39.37	42.00	40.63	40.42	40.67
H_2O	0.33	0.03	-	0.18	-	-	0.40	0.20	0.22
S	-	-	-	-	-	-	0.03	-	-
CO_2	-	1.10	-	-	0.30	-	1 .00	0.29	-
F	2.80	3.29	3.00	2.00	2.43	2.24	1.17	0.90	1 .06
Cl	-	0.03	-	0.40	0.15	-	-	-	-
SUM	100.07	100.88	101.38	99.81	99.98	100.82	100.92	100.27	100.07

Table 2. Symbols of sold solutions nAp(1-n)Wh , thermodynamic properties (in kcal) of the studied natural apatite (1-9) and crystallochemical formulas of the synthesized apatites (10-12) and whitlokite (13) in comparison with the reference data (14-16.)

	Formulas and symbols of solid solutions of apatites	$-\Delta H^{sol}_{343.15}$	$-\Delta H^{o}_{298}$	$-\Delta G^{o}_{298}$	S, cal
1	0.910 Ap·0.090 Wh	18.17±0.33	1603.00	1532.89	94.010
2	0.932 Ap·0.068 Wh	22.79±0.26	1590.82	1510.56	92.830
3	0.775 Ap·0.225 Wh	21.74 ±0.66	1575.76	1496.56	93.135
4	0.727 Ap·O.273 Wh	18.51±0.20	1625.90	1545.10	94.190
5	0.685 Ap·0.315 Wh	26.27±0.21	1600.61	1505.70	93.462
6	0.577 Ap·0.423 Wh	22.47±0.48	1585.90	1506.36	91.315
7	0.581 Ap 0.419 Wh	18.25±0.18	1566.10	1483.40	92.830
8	0.249 Ap 0.751 Wh	30.77±0.55	1504.78	1424.62	92.041
9	0.250 Ap·0.750 Wh	31.49±0.60	1512.48	1353.23	88.480
10	$Ca_5P_3O_{12}OH$	34.30±0.53	1609.15	1515.06	93.188
11	$Ca_5P_3O_{12}F$	15.80±0.30	1643.42	1563.57	95.700
12	$Ca_5P_3O_{12}Gl$	29.05+0.36	1584.72	1498.99	99.300
13	$Ca_{4.5}P_3O_{12}$	37.30±0.5	1473.44	1393.39	86.850
14	$Ca_5P_3O_{12}OH$	-	1606.50	1514.92	93.301
15	$Ca_5P_3O_{12}F$	-	1642.49	1555.48	92.701
16	$Ca_{4.5}P_3O_{12}$	-	1477.35	1396.63	84.602

The purity of the selected material was carefully controlled under a microscope. The chemical analysis was performed in the IEM RAS, in the laboratory of chemistry (Chernogolovka, Moscow distr.). and in SB RAS (Yakutsk). The concentration of fluorine was additionally analyzed by a method of channelling microanalyzer. The formulas in the form of apatite-whitlokite solid solutions nAp(1-n)Wh were calculated from the analyses. It can be seen from fig.1 that the compositions of apatites fit, in general, into the apatite-whitlokite series spanning it nearly completely. Determinations of dissolution enthalpy of natural and synthesized apatites were performed by the technique of [3]. The results of experimental measurements of dissolution enthalpy of apatites and calculated formation enthalpies of apatites using the schemes described earlier [4] are listed in table 2. For some apatites the low-temperature thermal capacities were measured on 400mg charges. A relative uncertainty of the measurements was 0.5%.

The diagram, fig.2., gives the comparison of the obtained results, including those for apatite solid solutions: hydroxylapatite-fluor(chlor) apatite and fluor(chlor) apatite-whitlokite. The latter substitution is energetically similar with substitution of fluorine by hydroxyl group.

An investigation of the isomorphous fluoroapatite-whitlokite series offers possibilities of thermodynamic calculation of their true stability at a significant deficiency of fluorine in the apatite composition.

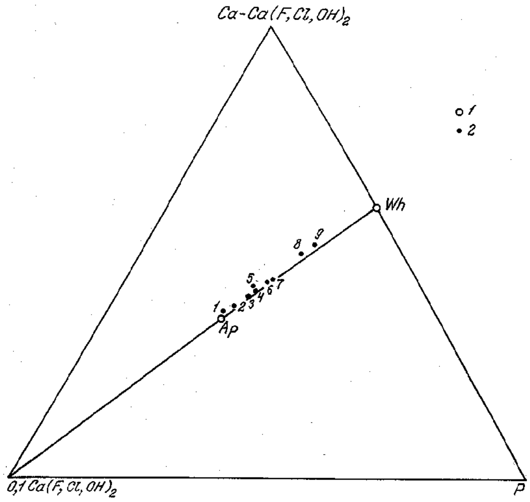

Fig.1. Position of thermochemically studied apatites on the diagram with respect to theoretical compositions of apatite (Ap) and whitlokite (Wt) 1-theoretical compositions; 2 - compositions of the analyzed apatites (from table 1)

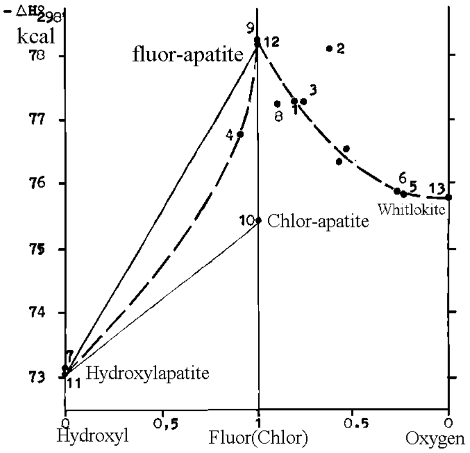

Fig.2. Change in the standard formation enthalpy (in kcal/at) of apatite in isomorphous hydroxyl-apatite-chlorapatite-fluoroapatite - whitlokite series (from the thermochemical data in table 2.)

References:

1. Vasil'eva Z.V. (1968) Mineralogic features and chemical composition of apatites. // Apatites, M., Nauka, pp.31-56.
2. Zinov'eva N.G., Mitreikina O.B. Granovsky L.B. (1997) Origin mechanism of hercynite-kamacite obiects: evidence for liquid immiscibility phenomena in the Yamato-82133 ordinary chondrite (H3)// Antartic meteorite Res., V.10, pp.299-311.
3. Marakushev A.A., Stolyarova T.A. (1998) Deficiency of volatiles in the apatite composition and thermochemistry of apatites. // Transact .Ac.Sci. V.363, N.6, pp.811-814.
4. Stolyarova T.A. Formation enthalpy of grossularite $Ca_3Al_2(SiO_4)_3$ in hydrofluoric acid. // Geochim., N.10, pp.1523-1526.

Aldushina E.A., Balitsky V.S., Chichagov A.V., Samokhvalova O.L., Bondarenko G.V. Synthesis of large crystals of sodium alumophosphate with the natisite structure and its structural and morphological characteristics.

key words: [*system, hydrothermal synthesis, natisite, sodium alumophosphate, X-ray diffraction, infrared spectroscopy*]

Various monocrystalline compounds are widely used in science and technics. Quartz and its structural analogues - berlinite and gallium orthophosphate, are the most important among them. In the laboratory of mineral synthesis and modifications of IEM the investigations of possibility of synthesis of crystals with mixed composition SiO_2-$AlPO_4$ are carried out. In this case, in the crystal forming system various accompanying phases form depending on solution composition and T-P parameters. The basic purpose of the study was synthesis and investigation of phases in the system $NaOH$-NH_4F-$AlPO_4$-H_2O.

Transparent pseudocubic light-green and prismatic colorless crystals of 0.5-7 mm in size were first synthesized. The study showed, that the obtained crystals were sodium alumophsphate $Na_3Al_2(F, OH)_3(PO_4)_2$, which corresponds to natisite structural type - $Na_2(TiO[SiO_4])$ [1].

Para-framework of mixed type, which can be described by the formula $(Al_2F_3[PO_4]_2)$ is built of Al-octahedrons and P-tetrahedrons connected by apexes. All apexes of the PO_4-tetrahedrons are shared with AlO_4F_2-octahedrons. The latter are combined in pairs in the direction of c-axis via apexes, which are occupied by atoms F1 in the inversion center. The second F-apex of each Al-octahedron is not shared with other polyhedrons in the framework structure. Therefore, framework structure transforms to pseudo-framework or para-framework. Cations Na^+ statistically occupy the cavities of the para-framework structure made of octahedrons and tetrahedrons.

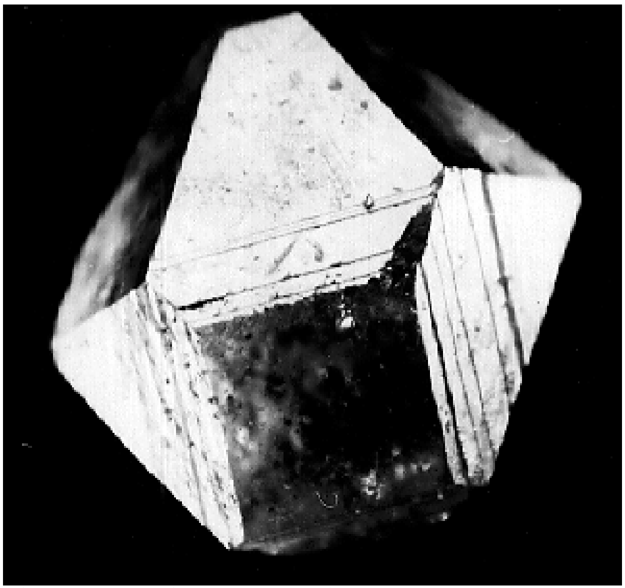

Fig.Pseudocubic crystal of $Na_3[Al_2(OH, F)_3(PO_4)_2]$, synthesized in the system $NaOH$-NH_4F-$AlPO_4$-H_2O. Cross size is 5 mm.

Growing the crystal of the synthetic sodium alumophosphate was performed by hydrothermal method. NaOH, $AlPO_4$, and NH_4F were used as starting substances. Different ratios of these components were used in different runs. Run duration varied from two weeks to one month. Temperature in the bottom of an autoclave was 300°C, in the top - 270°C; pH was above 10 in all runs.

Crystals of sodium alumophosphate (pseudocubic) were measured in two-circle reflecting goniometer. Quality of facets was perfect; hatchure, i.e. traces of undergrown layers, were locally observed; edges are straight and distinct.

Chemical composition of the synthesized samples was analyzed with CAMEBAX microprobe equipped with semiconductor defractormeter Link An 10000. Analysis was taken in 12 points of the crystal. Data, obtained for different areas of the sample, do not practically differ from each other. Analyses showed the presence of the following major chemical elements: Na - 17.927 wt %, Al - 13.79 wt %, P - 18.487 wt %. Indirect methods showed also oxygen (42.510 wt %) and fluorine in the sample.

Record of X-ray profiles was performed by «hybrid» autodiffractormeter. Step-by-step regime with $\theta = 0.01$ was applied. Angle positions of reflections were identified by the program Spectr-8. An accuracy was 0.01 degree. Angle positions of reflections were corrected according to external standard, which was silicon with parameter 5.4305 Å. Unit-cell parameters were specified from refinement of 18 reflections by least-square method with the program REFLAT. Specification showed the following unit-cell parameters: a = 6.1983 (0.0007) Å, c = 10.399 (0.001) Å.

Theoretical X-ray diagram was computed using the programs TRANS and XRAYPOL. Image was obtained with program the MIXPOL, included in the MINCRYST system. All obtained data are in a good agreement with the results of [2].

Spectrometer Perkin Elmer 983 was applied in the infrared spectroscopy. Infrared measurements were performed by the method of pressing KBr tablets (550 mg KBr per 2 mg of studied substance). Infrared spectra showed combination peaks of bonds in the PO_4-tetrahedron. Regions 1100 cm^{-1} - 1170 cm^{-1} were assigned to asymmetric valent bonds P-O, regions 700 cm^{-1} - to asymmetric deformational P-O, regions 470 cm^{-1} - to symmetric deformational P-O. Intensity and width of the peaks correspond to superposition of Al-O oscillations in a octahedron. Spectrum, obtained from a flat transparent plate cut from the crystal, showed the presence of intensive peaks of OH-groups in the region from 4000 cm^{-1} to 3000 cm^{-1}. Absence of deformation oscillations of water molecules in the region 1630 cm^{-1} shows, that oscillations in the region 3500 cm^{-1} correspond to OH-groups, exclusively.

The study of optical properties of sodium phosphate crystals by an immersion method showed, that the crystal is uniaxial, ordinary refractive index $n_0 \sim 1.529$, extraordinary $n_e \sim 1.538$.

Major results and conclusions

- The substance of a natisite structural type was first synthesized in the system $NaOH$-NH_4F-$AlPO_4$-H_2O.
- The synthesized substance is prismatic or pseudocubic transparent colorless or light-green crystals of 0.5 - 7 mm in size.
- On the basis of the study the synthesized substance is identified as sodium alumophosphate $Na_3Al_2(F, OH)_3(PO_4)_2$.
- Infrared spectroscopy allowed to identify OH-groups in the structure of the crystals.
- Optical constants and morphological characteristics of sodium alumophosphate are first described.
- On the basis of visual observations the domain structure of the crystals of sodium alumophosphate is assumed.

References:

1. Yakubovich O.V., Mel'nikov O.K., Urusov V.S. (1995) Para-framework of mixed nature in the crystal structure of

$Na_3[Fe_2F_3(PO_4)_2]$ - the new homeotype in the natisite structural type. //Doklady RAS, V.342, N. 5, pp. 616-620.

2. Yakubovich O.V., Mel'nikov O.K. (1996) Anionic framework of mixed type in the crystal structure of $Na_3[Al_2F_3(PO_4)_2]$. // Crystallography, V.41, N.4, pp. 663-668.

[#]Dorogokupets P.I., Ponomarev E.M., Melekhova E.A. Equation of state for minerals based on volume vs energy dependencies from Wachtman and Suzuki models.

key words [*equation of state volume heat capacity bulk moduli zoisite*]

For zoisite taken as an example we consider a simple thermal equation of state of minerals enabling us to simultaneously optimize experimental data on C_P, C_V, V, α, K_T at zero pressure and P-T data.Table 1**.** Calculated thermodynamic properties of zoisite, $Ca_2Al_3Si_3O_{12}(OH)$ using SW EoS at 0, 2, 4, 6 and 10 GPa

---

[#] The work was sponsored by the RFBR (Grant N 99-05-64891)

T	V	α	K_T	K_S	C_P	C_V	γ
(K)	(cm^3)	(K^{-1})	(GPa)		(J mol^{-1}K^{-1})		
			P=0 GPa				
100	135.829	7.901E-06	125.31	125.43	106.189	106.083	1.268
200	136.017	1.898E-05	124.83	125.43	255.776	254.553	1.266
298.15	136.319	2.576E-05	124.05	125.26	348.193	344.848	1.263
500	137.147	3.313E-05	121.96	124.50	450.646	441.465	1.255
1000	139.678	3.861E-05	115.74	121.24	531.036	506.938	1.231
1500	142.462	4.011E-05	109.21	117.12	555.861	518.321	1.204
			P=2 GPa				
100	133.733	7.320E-06	130.79	130.91	102.727	102.633	1.248
200	133.906	1.785E-05	130.33	130.91	251.081	249.969	1.246
298.15	134.187	2.435E-05	129.58	130.75	343.624	340.550	1.243
500	134.959	3.148E-05	127.56	130.04	446.993	438.462	1.236
1000	137.330	3.680E-05	121.50	126.92	528.540	505.946	1.214
1500	139.938	3.820E-05	115.10	122.94	553.276	518.010	1.188
			P=4 GPa				
100	131.751	6.810E-06	136.15	136.26	99.516	99.433	1.229
200	131.912	1.684E-05	135.71	136.27	246.655	245.640	1.227
298.15	132.173	2.309E-05	134.99	136.13	339.304	336.466	1.225
500	132.897	3.001E-05	133.03	135.46	443.526	435.567	1.218
1000	135.126	3.518E-05	127.12	132.47	526.233	504.973	1.197
1500	137.578	3.651E-05	120.86	128.62	550.946	517.697	1.173
			P=6 GPa				
100	129.873	6.359E-06	141.39	141.50	96.527	96.453	1.211
200	130.022	1.594E-05	140.97	141.52	242.473	241.542	1.209
298.15	130.266	2.197E-05	140.28	141.39	335.208	332.578	1.207
500	130.946	2.868E-05	138.38	140.76	440.226	432.775	1.201
1000	133.049	3.373E-05	132.61	137.89	524.088	504.018	1.181
1500	135.362	3.500E-05	126.47	134.16	548.833	517.383	1.158
			P=10 GPa				
100	126.385	5.597E-06	151.56	151.66	91.122	91.062	1.177
200	126.514	1.439E-05	151.17	151.69	234.742	233.950	1.176
298.15	126.731	2.002E-05	150.53	151.59	327.601	325.321	1.174
500	127.337	2.638E-05	148.74	151.03	434.057	427.469	1.169
1000	129.225	3.122E-05	143.23	148.38	520.196	502.159	1.151
1500	131.303	3.239E-05	137.34	144.88	545.129	516.752	1.130

The volume vs energy dependence in the models of Wachtman et al (1962) and Suzuki (1975) can be extended to high pressures. The basic calculation formulas are given below, and their more detailed description is given in [Dorogokupets et al, 1998,Dorogokupets et al 1999, Dorogokupets 1999]. They are valid for minerals with the unknown dependence of the bulk moduli on temperature.

$$V_{PW} = V_{P298}[\Delta E_P/(\frac{V_{P298}K_{PT298}}{\gamma_{P298}} - \frac{K'_P-1}{2}\Delta E_P)+1],$$

$$V_{PS} = V_{P298}[K'_P - (1-\frac{2\gamma_{P298}(K'_P-1)\Delta E_P}{V_{P298}K_{PT298}})^{0.5}]/(K'_P-1),$$

$$V = V_{PW}(1-X) + V_{PS}X,$$

$$E = 0.75nR\Theta(\frac{1}{e^{\Theta_1/T}-1}+\frac{0.5}{e^{\Theta_1/2T}-1}+\frac{1}{e^{\Theta_2/T}-1}+\frac{0.5}{e^{\Theta_2/2T}-1})$$

$-a_oT^2(V/V_{298})$, a_o and X are empiric parameters

$$C_P = C_V + \alpha^2 VTK_T,$$

$$K_T = K_S - VT(\alpha K_T)^2/C_V,$$

$$P = 3fK_T(1+2f)^{5/2}(1+af),$$

$$K_T = K_{T298}(1+2f)^{5/2}[1+(7+2a)f+9af^2],$$

$$K'_T = [12+2a+(49+32a)f+81af^2]/\{3[1+(7+2a)f+7af^2]\},$$

$$f = 0.5[(V_{T,P}/V_T)^{-2/3}-1],\ a=1.5(K'-4),$$

$$P_{V,T} = P_{VTo} + \frac{\gamma}{V}\Delta E_{VT},$$

$$\Theta_i = \Theta_i \exp(\frac{\gamma_{298}-\gamma}{q}),\quad \gamma = \gamma_{298}(V/V_{298})^q.$$

The fitting parameters of the model are: volume, V_{298}, Nernst-Lindemann temperature, $\Theta=(\Theta_1+\Theta_2)/2$, isothermal bulk modulus, K_{T298}, its pressure derivative, K', Gruneisen parameter, γ_{298}, and the complementary empiric parameter a_o that can be zero for minerals with simple structure (Debye-like solids). This formulation is one of the versions of the Mie-Grűneisen equation. The equation of state can be represented both in the classic form MGEoS and via volume vs temperature on isobars by Wachtman and Suzuki models, SW EoS.

We know for zoisite the heat capacity from [Kiseleva et al, 1974, Perkins et al, 1980] and one determination of volume vs temperature (Pawley et al, 1996) at zero pressure. The PVT data for zoisite from the works (Holland et al, 1996, Comodi, Zanazzi, 1997; Pawley et al., 1998; Grevel et al., 1999) are conflicting due both to the sample origin and methodical reasons. The joint data processing (Perkins et al., 1980; Pawley et al., 1996; Comodi, Zanazzi, 1997; Pawley et al., 1998; Grevel et al., 1999) yields the following fitting parameters: V_{298} = 136.32 cm^3, Θ_1 = 1445 K, Θ_2 = 517 K, K_{T298} = 124.05 GPa, K' = 2.8, γ_{298} = 1.263, X = 0, a_o = –5.33E–3 J K^{-2}. The parameter q is taken to be unity. V_{298} was derived from the data(Pawley et al., 1996), the remaining $P–V–T$ data were normalized to V/V_{298}. An uncertainty of C_P approximation is ±2.4 J mol^{-1}K^{-1}, of the $P–V–T$ data (Grevel et al., 1999) ±0.34 GPa, of the data (Pawley et al., 1998) ±0.33 GPa and of the data (Comodi, Zanazzi, 1997) ±0.22 GPa. These parameters were used to calculate the thermodynamic functions of zoisite from the models of Wachtman and Suzuki (SW EoS) on different isobars (Table 1). Fig.1. illustrates the heat capacity of zoisite in comparison with the other data, fig.2 illustrates the volume of zoisite.

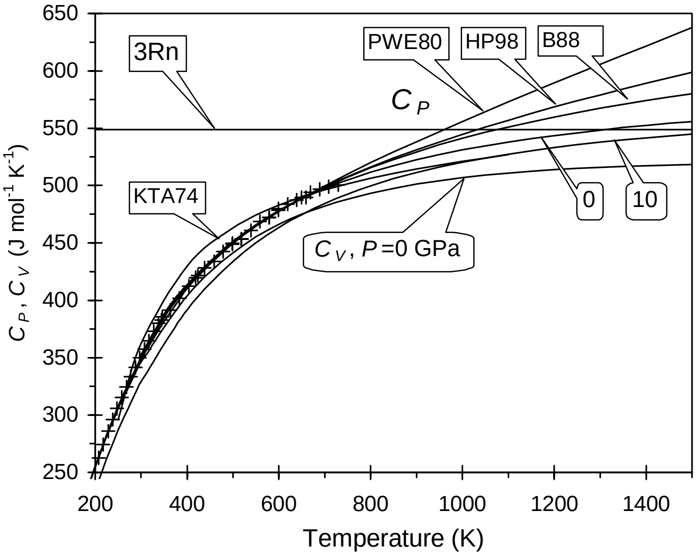

Fig.1. Calculated isobar (at 0 and 10 GPa) and isochor heat capacity of zoisite. 3Rn is high temeprature limit of Debye heat capacity, PWE80- Perkins et al (1980; HP98-Holland and Powell (1998)); B88 - Merman (1988); KTAZ4 - Kiseleva et al (1975).

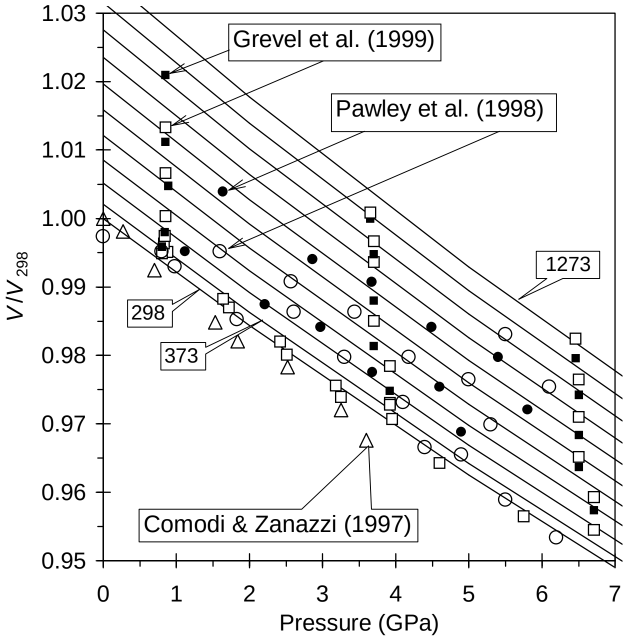

Fig.2. Calculated volume of zoisite on isotherms in 100 K intervals, compared to experimental data.

Close values of K_{T298} and K' can be obtained by using the technique of P-V-T data processing of (Grevel et al., 1999) with allowance for the weights, we obtain: V_{298} = 900.83 Å^3, K_{T298} = 133.2 GPa, K' = 1.47, $(\partial K_T/\partial T)_V$ = –0.02 GPa/K. All the parameters are fitting here and standard uncertainty σ is 0.25 GPa. With three fitting parameters when thermal pressure is volume-independent, we have: V_{298} = 900.38 Å^3, K_{T298} = 142.0

GPa, $K' = -0.43$, $\sigma = 0.26$ GPa. Similarly, from the data of (Pawley et al., 1998) we obtain: $V_{298} = 907.93$ Å^3, $K_{T298} = 174.3$ GPa, $K' = -9.24$, $(\partial K_T/\partial T)_V = 0.04$ GPa/K, $\sigma = 0.25$ GPa, and $V_{298} = 908.45$ Å^3, $K_{T298} = 159.7$ GPa, $K' = -6.76$, $\sigma = 0.26$ GPa, i.e. here we also have conflicting results. We, however, mention that in the work (Grevel et al., 1999), three series of measurements were conducted each of which yielded different values of zoisite volume under standard conditions. If one calculates from them the V/V_{298}, values, which seems more reasonable than using the fitting V_{298} value, then with three fitting parameters we obtain: $K_{T298} = 126.5$ GPa, $K' = 2.98$, $(\partial K_T/\partial T)_V = -0.018$ GPa/K, $\sigma = 0.23$ GPa and with two: $K_{T298} = 131.0$ GPa, $K' = 1.79$, $\sigma = 0.26$ GPa. If we take $K' = 2.98$, then from the data of (Pawley et al., 1998) we obtain: $V_{298} = 909.46$ Å^3, $K_{T298} = 123.2$ GPa, $\sigma = 0.32$ GPa and with $K' = 1.79$ we have $V_{298} = 909.33$ Å^3, $K_{T298} = 126.9$ GPa, $\sigma = 0.31$ GPa. Comodi and Zanazzi (1997) obtained on room isotherm $K_{T298} = 102 \pm 6.5$ GPa and $K' = 4.8 \pm 0.4$, whereas according to Holland et al. (1996) we have $K_{T298} = 279 \pm 9$ GPa at $K' = 4$.

References:

1. Berman R.G. (1988). J. Petrol., 29, 445–522.
2. Comodi, P. and Zanazzi, P.F. (1997). Amer. Mineral., 82, 61-68.
3. Dorogokupets P.I. (1999). Amer. Mineral. (In press).
4. Dorogokupets P.I., Ponomarev E.M. (1998). Exp. in Geosciences, 1998, Vol. 7, 73-75
5. Dorogokupets P.I., Ponomarev E.M., Melechova E.A. (1999). Petrology, 7(6).
6. Grevel K.-D., Nowlan E.U., Fasshauer D.F., Burchard M. (1999). Amer. Mineral. (In press).
7. Holland T.J.B., Powell R. (1998). J. Metamorphic Geology, 16, 309-343.
8. Jackson I., Rigden S.M. (1996). Physics Earth Planet. Inter., 96, 85–112.
9. Kiseleva I.A., Topor N.D., Andreenko E.D. (1974). Ceokhimia, No. 4, 543-553.
10. Pawley, A.R., Chinnery, N.J., and Clark, S.M. (1998). Amer. Mineral., 83, 1030-1036.
11. Pawley A.R., Redfern S.A.T., Holland T.J.B. (1996). Amer. Mineral., 81, 335–340.
12. Perkins D., III, Westrum E.F., Jr., Essene E.J. (1980). Geoch. Cosmoch. Acta, 44, 61–84.
13. Suzuki I. (1975). J. Physic Earth, 23, 145–159.
14. Wachtman J.B., Scuderi T.G., Gleek G.W. (1962). J. Amer. Ceramic Society, 45, 310–323.

[#]Ogorodova L.P., Melchakova L.P., Kiseleva I.A. Calorimetric study of natural epistilbite.

key words [*zeolite epistilbite calorimetry heat capacity enthalpy dehydration*]

A sample of natural zeolite of the mordenite group-epistilbite $(Ca_{0.80}Na_{0.34}K_{006})[Al_{1.97}Si_{6.01}O_{16}]\cdot 5.10H_2O$ (Berufjord Iceland) was studied chemically and by X-rays. Its behaviour upon heating was examined by thermal thermogravimetric analyses (DTA, TG, DTG) (Derivatograph Q-1500 D). Epistilbite is stable to T=323K, its dehydration proceeds in three stages and accomplished at T=823K.

Heat capacity measurements were conducted on a differential scanning calorimeter DSC "Mettler TA-2000B" in the range of T=110-320 T in flowing nitrogen at a scanning rate of 5-10k/min. The calibration was performed with respect to heat and melting temperature of the reference - metalic indium (99.9999% pure). A small anomaly was observed in the heat capacity of epistilbite in the range of 120-200K that is, possibly, related to proton disordering, by analogy with such having found by us earlier in zeolites (gonnardite, thomsonite, and edingtonite). The derived value $C^o_p(298.15)=665.9$ J/mol·K agreed within our experimental uncertainties (±1-1.5%) with the results of [1] obtained on a sample of the same composition by adiabatic calorimetry method (660.3±0.6 J/mol·K).

The enthalpies of dehydration and formation were defined on a high-temperature heat-flux Calvet microcalorimeter. The process of dehydration of epistilbite was studied by a "double drop" method. The zeolite sample was first dropped from room temperature into a calorimeter the temperature of which was 973 K (higher than the dehydration temperature), and the heat effect was measured associated with the sample heat absorption and the process of its dehydration at T=973K, $\Delta H^o_{drop\ deh}(973) = 872.2 \pm 9.2$ kJ/mol. The solid dehydration product was then dropped again into the calorimeter and the enthalpy gain of the dehydrated sample was measured $\Delta H^o_{drop}(973) = 364.0 \pm 8.3$ kJ/mol. The amount of the released water (15.0%) was defined by weighing the sample before and after the run with an accuracy of $\pm 2 \cdot 10^{-3}$ mg. The dehydration enthalpy of epistilbite, calculated from the experimental data, was $\Delta H^o_{deh}(298.15) = 156.6 \pm 12.4$kJ per 5.10 moles of water, which corresponds to the heat effect of about 30 kJ/mol were obtained for other zeolites of the mordenite group, i.e. bikitaite and mordenite.

The enthalpy of formation was defined by a method of high temperature solution calorimetry in a $2PbO\cdot B_2O_3$ melt at T=973K. The run was conducted by a transposed temperature drop solution method. Thereat combined measurements of the zeolite enthalpy gain and its dissolution enthalpy at T=973K were performed, $\Delta H^o_{drop\ sol}(973) = 681.6 \pm 8.5$ kJ/mol. The enthalpy of formation of epistilbite from oxides was calculated using the values of dissolution enthalpies and heat contents of the epistilbite constituent oxides: $\Delta H^o_{f\ ox}(298.15) = -116.0 \pm 18.0$ kJ/mol. The enthalpy of formation of epistilbite from the elements was defined with account taken of the reference data [2] on enthalpies of formation of the constituent oxides to be $\Delta H^o_{f\ ox}(298.15) = -9286.0 \pm 19.0$ kJ/mol. Using the results of determination of $S^o(298.15)$ of epistilbite of the same composition [1] and the reference data on standard entropies of elements at T=298.15 K [2] we calculated the value of $\Delta G^o_f(298.15)$ of epistilbite to be -8568.6 ± 19.0 kJ/mol.

References:

[#] The work has been sponsored by the RFBR (Project N 97-05-64805) ·

1. Paukov I.E., Belitsky I.A., Berezovsky G.A. (1998) Thermodynamic properties of natural zeolite-epistilbite. // Geochim., N.6, pp.638-643.
2. Robie R.A., Hemingway B.S. (1995) Thermodynamic properties of minerals and related substances at 298.15K and 1 bar (105 Pa) pressure and a higher temperatures. // US Geol. Surv. Bull, N.213, 462p.

[#]Ogorodova L.P., Kovalskii A.M., Kotel'nikov A.P. Thermochemic investigation of (Sr, Ba) feldspar solid solutions.

key words [*feldspar solid solutions synthering unit-cell parameters thermochemic investig*ation]

Synthesis of (Sr,Ba)-feldspar solid solutions was performed by two techniques:

1) synthering from a mixtures of carbonates and oxides under dry conditions (T=1480°C, the run duration was 48h);

2) hydrothermal recrystallization of the synthering products (T=700°C, P_{H2O}=2 kbar, the run duration was 264h).

The starting materials were mixtures of carbonates and oxides ($BaCO_3$, $SrCO_3$, Al_2O_3, SiO_2) taken in stoichiometric ratios. The compositions of feldspars synthesized by the both techniques correspond to stoichiometry of the minerals of the $(Sr,Ba)Al_2S_2O_8$ series.

<u>X-ray study of (Sr,Ba)-feldspars.</u> X-ray analysis of the synthesized samples showed that they were homogeneous and highly crystallized. The unit cell parameters were therefore refined for solid-solution series. The samples were photographed in the mode of continuous scanning of the total X-ray diffraction profile on an automated diffractometer PS/HZG-4. Angular positions of the reflexes were estimated by the program Spectr-8 (Okhulkov A.V., IEM, RAS) and adjusted for the internal standard (Si of spectral purity, a=5.4305Å). The unit cell parameters were refined by using, on average, 30-40 reflexes in the angle range of 7-39 degrees (Θ). Computer programs LCC, PUDU [1,2] were used for the refinement. The computed values of the unit-cell parameters of (Sr, Ba)-feldspars at 20°C are listed in table 1. The parameter values obtained in the works of Nager [3], Chernysheva et al [4] fairly agree with our results.

[#] The work was sponsored by the RFBR (Project N 97-05-65886)

Table 1. Unit-cell parameters of (Sr, Ba)-feldspars

X_{Ba}^{Fsp}	a,[Å]	b[Å]	c,[Å]	β[°]	V, [Å^3]	Footnote
0.00	8.385(1)*	12.968(1)	7.131(1)	115.37(1)	700.7(1)	1-1
0.00	8.393(1)	12.972(1)	7.131(1)	115.40(1)	701.3(2)	1-2
0.19	8.437(1)	12.986(1)	7.139(1)	115.27(1)	707.3(2)	1-1
0.21	8.437(2)	12.988(1)	7.146(2)	115.33(1)	707.8(3)	1-2
0.45	8.501(1)	12.998(1)	7.163(1)	115.16(1)	716.4(2)	1-1
0.49	8.509(1)	13.001(1)	7.163(1)	115.15(1)	717.3(3)	1-1
0.52	8,516(2)	13.005(2)	7.169(1)	115.17(1)	718.6(2)	1-2
0.58	8.535(1)	13.011(2)	7.166(1)	115.09(1)	720.7(2)	1-1
0.61	8.537(1)	13.014(1)	7.174(1)	115.15(1)	721.5(2)	1-2
0.80	8.598(1)	13.035(1)	7.185(1)	115.08(1)	729.3(2)	1-1
0.83	8.587(1)	13.031(1)	7.188(1)	115.14(1)	728.1(1)	1-2
1.00	8.642(1)	13.049(1)	7.204(1)	115.17(1)	735.2(1)	1-1
1.00	8.637(1)	13.049(1)	7.207(1)	115.18(1)	735.1(2)	1-2

*the uncertainties of the unit-cell parameters refinements are given in brackets and are pertinent to the last decimal places; 1-1 the samples, synthesized by solid-state synthesis from mixtures of oxides and carbonates at 1480°C; 1-2 solid solutions, produced by hydrothermal treatment (700°C, P_{H2O}=2 kbar, run duration 264h) of 1-1 series samples.

Table 2. Experimental values of enthalpies of dissolution of (Sr,Ba)$Al_2Si_2O_8$ solid solutions in molten 2PbO·B_2O_3 at 973K.

	ΔHsol,973 (kJ/mole)	
X_{Ba}^{Fsp}	Samples produced by synthering at 1480°C	Hydrothermally decrystallized synthering products
0.0	87.02 ± 2.49 (6) (run 4713)	84.4 ± 6.1(4) (run 4736)
0.19	92.46 ± 1.68 (6) (run 4715)	-
0.49	97.91± 4.33 (4) (run 4717)	-
0.52	-	101.4(2) (run 4738)
0.8	103.45 ± 2.20 (5) (run 4719)	-
1.0	110.27 ± 7.38 (6) (run 4714)	117.2±5.3(3) (run 4737)

The mixing volumes of (Sr, Ba)-feldspars obey Vegard rule, respectively, excess volumes of mixing are zero.

Thermochemical investigation of (Sr, Ba)-feldspars. Thermochemical investigation was performed in the laboratory of experimental thermodynamics of minerals, dep. of geology, Moscow State University on a Calvet high- temperature differential microcalorimeter ("Setaram", France) using a method of drop-solution in molten 2PbO·B_2O_3 at T=973 K[5]. The calorimeter was calibrated for the reference H^o_T-H^o_{298} value of the standard material-platinum [6]. The sample weighing was performed with an accuracy $\pm 2\cdot 10^{-6}$ g. High-crystalline and homogeneous samples of feldspars were taken for the thermochemical investigation. The calorimetric measurements yielded the enthalpies of dissolution of (Sr,Ba)-feldspar solid solutions :

1. produced by synthering (with X_{Ba}^{Fsp} = 0.00; 0.19; 0.49);
2. recrystallized under hydrothermal conditions (with X_{Ba}^{Fsp} = 0.00; 0.52; 1.00).

The results of the thermochemical investigations of $BaAl_2Si_2O_8$ - $SrAl_2Si_2O_8$ are listed in table 2 and illustrated in fig.1.

As seen from the figure, the obtained enthalpies of dissolutions are well described by linear dependences within the measurement uncertainties.

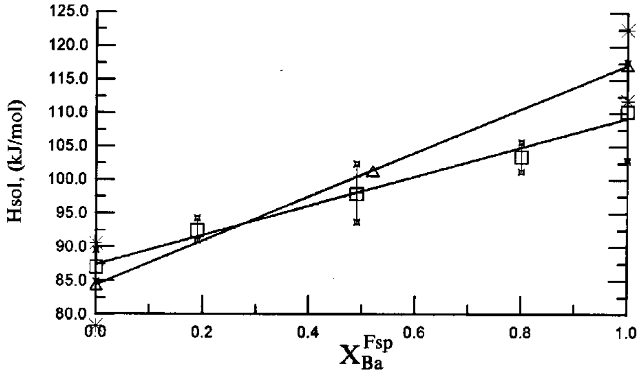

Fig.1. Concentration dependences of enthalpies of dissolution of (Sr,Ba)-feldspar solid solutions produced by two methods: -synthering from mixtures of oxides and carbonates ; Δ - hydrothermal recrystallization of synthering

products. The dimensions of the vertical lines correspond to uncertainties of determination of dissolution enthalpies.

References:

1. Burnham C.W. (1962) IBM computer program for least-squares refinement of crystallographic lattice constants. Geophys. Lab. Carnegie Inst. Washington, D.C., Yearbook, , v. 61,p. 132-135.
2. Burnham C.W. (1991) Least-squares refinement of crystallographic lattice parameters for IBMPC/XT/AT and compatibles, Harward University, Cambridge MA02138, (programdescription, 24p.).
3. Nager H.E. (1974) Gitterkonstanten und displasive Transformation von synthetischenFeldspaten im system (Ca,Sr,Ba)Al2(Si,Ge)20g. Inaug. Dissert., Munster, 189 p.
4. Chernysheva I.V., Urusov V.S., Semenov Yu.V., Kuznetsova T.P. (1991) Isomorphism and properties of mixing of Ca-Sr-, Sr-Ba, Ca-Ba-feldspar solid solutions. // Vestnik Mosk. Univ., ser. geol., V.46, N.1, pp.44-54.
5. Kiseleva I.A., Ogorodova L.P., Topor N.D., Chigareva O.G. (1979) Thermochemical investigations in the Cao-Mg0system. // Geochim., N.12, pp.1811-1825.
6. Robie R.A., Hemingway B.S., Fisher J.R. (1978) Thermodynamic properties of minerals andrelated substances at 298.15 K and 1 bar pressure and at higher temperatures.U.S.Geol.Surv.Bull., N1452, 456 p.

#Mel'chakova L.V., Ogorodova L.P., Kiseleva I.A. Thermochemic study of tungstite $WO_3 \cdot H_2O$.

key words [*tungstite calorimetry heat capacity entropy*]

A thermodynamic approach to the description of the physicochemical conditions of tungsten transport in hydrothermal solutions requires reliable thermodynamic constants of minerals, tungstite $WO_3 \cdot H_2O$ included.

A thermodynamic analysis was performed on a synthetic analog of tungstite - commercial product of high purity, tungstic acid. The powder X-ray diffraction data showed that the used material was identical with the tungstite mineral (database ICPDS).

The thermal and thermogravimetric analyses showed that tungstic acid was stable to T=350K. Water loss occurs in three stages ceasing at T=900K. The heat capacity in the range T=110-340K was measured on a differential scanning calorimeter crucibles in flowing nitrogen. 5 run series were conducted both in heating mode at a rate 10°/min and cooling mode at a rate 5°/min. The instrument was calibrated with respect to temperature and melting heat of the reference material, i.e. metallic indium (99.9999% pure).

The results of the heat capacity determinations at T=290-340K (prior to the temperature of the material decomposition) were used to calculated the dependence of heat capacity of tungstic acid on temperature: $C^o_p=92.0+110.0 \cdot 10^{-3}$ T J/mol·K in the range of T=298.15-340 K, $C^o_p(298.15)=124.8$ J/mol·K.

The results of the runs at temperatures below room temperature (110-300K) were levelled, and the extrapolation was performed towards lower temperature region to T=0 K by means of the Debye function. The characteristic temperature (Θ_D=719 K) was estimated from the experimental values of heat capacity of tungstic acid at T=110-130K. Numerical integration of the C^o_p=f(T) and C^o_p/T=f(T) functions were used to calculate the gain $H^o_{298.5}-H^o_o=19829.4$ J/mol and the entropy gain $S^o_{298.5}=106.8$ J/mol·K.

The enthalpy of formation of tungstic acid from the elements was calculated by us earlier on the base of the available published calorimetric data on dissolution of tungsten trioxide and tungstic acid in alkali solutions. It equalled $\Delta H^o_{,\ f298.15}= -269.5 \pm 0.2$ kcal/mol = -1127.6 ± 0.8 kJ/mol.

Based on that value of enthalpy of formation and here obtained entropy, we calculated the value of free energy of formation of tungstic acid from the elements to be $\Delta G^o_{,\ 298.15}=988.5$ kJ/mol.

Reference:

1. Kiseleva I.A., Ogorodova L.P., Khodakovsky I.L. (1980) Thermodynamic properties of scheelite and tungstate - ion. // Geochim., N.8, pp.1123-1129.

#Kiselyova I.A., Ogorodova L.P., Mel'chakova L.V. Synthesis and thermal stability of tungsten heteropolycompounds.

key words [*tungsten heteropolycompounds, thermal analysis, thermal stability, decomposition temperature*].

It is known, that tungsten in hydrothermal aqueous solutions can form various polynuclear complexes, which are presented by iso- and hetropolycompounds. This fact led many investigators to idea of possibility of tungsten transport in complex polymeric species (heteropolycompounds) [1, 2]. Equilibrium between mono- and polymeric tungsten species depends on pH of a solution, total tungsten concentration, and temperature. Interest in heteropolycompounds, both crystalohydrates and aqueous solutions, is also related to their using as independent heterogeneous catalysts, as well as starting material for production of the compounds, containing catalyticaly active centers [3].

We undertook the thermal and thermogravimetric study of two heteropolycompounds of tungsten, containing phosphorus and stibium.

Synthesis was carried out by the method of co-precipitation in acid solution of sodium tungstate. The obtained heteropolycompounds in saturated aqueous solutions form highly aqueous crystalohydrates of the following compositions: $Na_3[PW_{12}O_{40}]*30H_2O$ and

---

The work was performed under the Program "Universities of Russia - Fundamental researches"

The study was fulfilled under support of the program "Universities of Russia - fundamental investigations".

$Na_6[HSbW_{11}O_{38}]*14H_2O$. Water content was identified with accuracy ±$2*10^{-3}$ mg by weighing the samples before and after annealing.

The synthesized phases were studied by the methods of differential thermal analysis (DTA) and thermogravimetric (TG) analysis using Derivatograph Q-1500 D (Hungary) within the interval 20 - 1000^OC, as well as using differential scanning calorimeter (DSC "Mettler TA-2000 B", Swizerland) within the interval from -170 to 550^OC.

It is found, that tungsten-phosphorus crystalohydrate of the 12-th sequence $Na_3[PW_{12}O_{40}]*30H_2O$ in dynamic regime of heating with a rate of 20 ^{O}/min shows water loss beginning from 50^OC and proceeding in three stages. The first occurs in the interval 50-250^OC with T_{max} = 160^OC and is characterized by the loss of about 26 moles of water. The second stage (250 - 360^OC) is accompanied by the loss of 3 moles of water. During the third stage the gradual loss of the last 1 mole of water in the interval 360 - 600^OC is observed. The process of heteropolycompound decomposition occurs at 620^OC, forming non-volatile products (WO_3, Na_2WO_4 etc.) and being accompanied by exothermic effect. Enthalpy of dehydration (loss of the major portion of water, i.e. 29 moles) on the first stage (690 kJ/mol) and the second stage (213 kJ/mol) were measured with DSC. This corresponds to endothermic effect of the loss of 1 mole of water - 27 kJ/mol and 71 kJ/mol, respectively. The study of sodium tungsten-phosphate at temperatures below the room temperature (down to -170^OC) did not show the presence of phase transitions.

The study of thermal behavior of crystalohydrate $Na_6[HSbW_{11}O_{38}]*14H_2O$ by DTA and TG in the dynamic regime with a rate of 20^O/min showed, that dehydration process proceeded in three stages: in the interval 50 - 260^OC (loss of 10 moles of water), in the interval 260 - 600^OC (2.5 moles of water), and in the interval 340 - 580^OC (1.5 moles of water). The stages are followed by the complete decomposition of the heteropolycompound with formation of volatile phases, accompanied by some weak endo- and exothermal effects.

High volatility of Sb-bearing tungsten heteropolycompounds allows to assume the possible participation of such complexes in the transport of tungsten by pneumatoliths.

References:

1. Gundlach H., Thormann W. (1960) Zeitschr. Fur der Deutsch Geol. Geselshaft, Bund 112, 1.
2. Ivanova G.F. (1972) Geochemical conditions of the formation of tungsten ore deposits. //Moscow. Nauka, 150 p.
3. Yurchenko E.N. (1986) Methods of the molecular spectroscopy in the chemistry of coordination compounds and catalysts. // Novosibirsk, Nauka, 252 p.

Priemysheva M.N., Gurevich V.M., Khodakovsky I.L. Thermodynamic properties of strontianite $SrCO_3$ and celestine $SrSO_4$

key words [*thermodynamic properties strontianite $SrCO_3$]celestine $SrSO_4$ entropy thermal capacity*]

Strontianite and celestine are ore forming minerals in sedimentary strontium deposits. A study of thermodynamic properties of these substance is therefore of considerable interest for a large number of researchers: geologists, geochemists, and chemists. Recently compounds of strontium have drawn the attention of ecologists in connection with studies concerned with rehabilitation of areas polluted with radioactive isotopes of this element.

The goal of this work is to correlate such dissimilar experimental data as C_p and $H^o_T - H^o_{298.15}$ for $SrCO_3$ and $SrSO_4$ and to define the coefficients in the equations of the temperature dependence of heat capacity at T>298.15K.

The standard values of heat capacity and entropy of strontianite, cited in reference books, are based on Anderson's measurements [1] of heat capacity of natural strontianite (containing 7% $CaCO_3$ as impurity) in the temperature range of 54.7–291.2 *K,* and the equation of the temperature dependence of heat capacity is based on the measurements of $H^o_T - H^o_{298.15}$ in the temperature range of 456–1323.6 *K* performed by Lander [2].

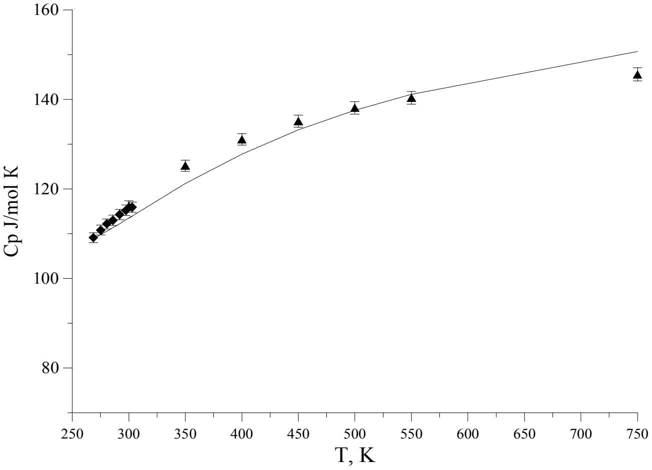

Fig.1.Temperature dependence of heat capacity

Recently, based on heat capacity measurements data obtained for strontianite $SrCO_3(k)$ by an adiabatic calorimetry method in the temperature range of 22.13-336.94K [3], standard values of heat capacity and entropy of this mineral were obtained to be: $C_p{}^o{}_{298.15K} = 86.52 \pm 0.15$ J·mol^{-1} K^{-1}, $S^0{}_{298.15\,K} = 100.01 \pm 0.24$ J mol^{-1} K^{-1}, and in [4] its enthalpy was defined by a drop method on a Tian-Calvet microcalorimeter at 973.15K.

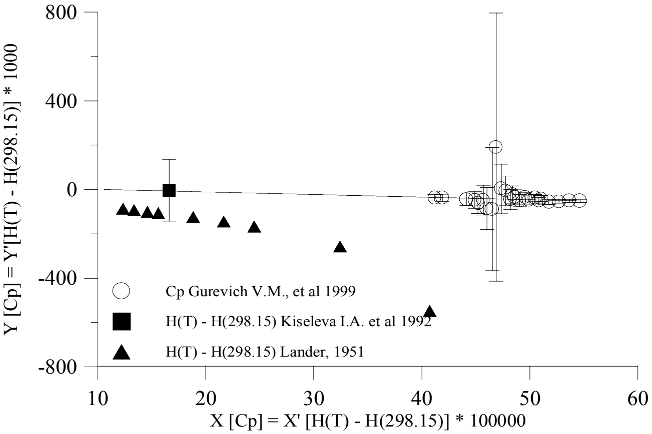

Fig.2. Correlation of dissimilar thermodynamic data (C_p and $H^o{}_T - H^o{}_{298.15}$ for $SrCO_3$

V.M.Gurevich et al [7] using a method of adiabatic calorimetry were the first to measure low-temperature heat capacity of strontianite Sr $SO_4(k)$ in the range 9.49-302.96K. They determined standard values of heat capacity and entropy of this mineral to be $C_p{}^o{}_{298.15\,K} = 115.09 \pm 0.33$ J·mol^{-1} K^{-1}, $S^0{}_{298.15\,K} = 135.01 \pm 0.25$ J mol^{-1} K^{-1}.The authors of [8] also measured for the first time high-temperature heat capacity of celestine within 280-800K by a method of differential scanning calorimetry and its enthalpy ($H^o{}_T - H^o{}_{298.15}$) by a drop method an a Tian-Calvet microcalorimeter at 973.15K.

The method of correlation of dissimilar experimental data (C_p and $H^o{}_T - H^o{}_{298.15}$), proposed by I.L.Khodakovsky in [9] was used to define (figs 2,3) the empiric coefficients in the equations of the temperature dependence of heat capacity for $SrCO_3$ and $SrSO_4$ (in excess of the upper temperature of the "anomalous" heat capacity zone equal to 268.75K)

for $SrCO_3(k)$:

$$Cp = 15R\ (1 - 115.933\ T^{-1} + 5115.315\ T^{-2}) + 0.0117T \qquad (1)$$

and for $SrSO_4(k)$:

$$Cp = 18R\ (1 - 52.711\ T^{-1} - 7872.37\ T^{-2}) + 0.0173\ T \qquad (2)$$

where R = 8.31441. The equations (1) and (2) are recommended for calculation of thermodynamic properties of these minerals at elevated temperatures.

The standard values of heat capacity and entropy of celestine, cited in reference books, were borrowed mainly from the works of Sakamoto [5-6] who calculated C_p of strontium sulfate by a method of estimation using the data on heat capacity of $BaSO_4$ and $CaSO_4$, studied experimentally.

The equations of the temperature dependence of heat capacity of celestine at T>298.15K were based on estimations.

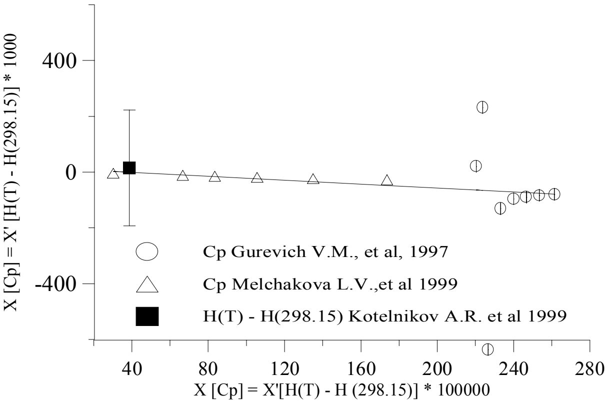

Fig.3. Correlation of dissimilar thermodynamic data (Cp and $H^o{}_T - H^o{}_{298.15}$ for $SrSO_4$)

References:

1. Anderson.C.T. (1934) // J.Amer.Chem.Soc., 56, 849, 340-342.
2. Lander, J. J. (1951) // J.Amer.Chem.Soc., 73, 5794.
3. Gurevich V.M., Gavrichev K.S., Gorbunov V.E., Danilova T.V., Golushina L.N., Khodakovsky I.L. (1999) // Geochim., to be published.
4. Kiseleva I.A., Ogorodova L.P., Kotelnikov A.R. (1992) // Geochim, pp.139-144.
5. Sakamoto Y. // J. Sci. Hiroshima Univ. Ser. A. V. 17. N 3. 397-405 (1954).
6. Sakamoto Y. (1954) // J. Sci. Hiroshima Univ. Ser. A. V. 17. N3, 407-411.
7. Gurevich V.M., Gavrichev K.S., Gorbunov V.E., Danilova T.V, Khodakovsky I.L. (1997) // Geochim., N 3, 305-311.
8. Kotelnikov A.R. et al (1999)// Geochim., to be publihed.
9. Khodakovsky I.L. (1975 //Physiko-khimicheskie Problemy Gidrotermal'nykh i Magmaticheskikh Protsessov, Nauka, Moscow, 124-150.

Pozhidaeva O.V., Varlamova O.E., Korytkova E.N. and Gusarov V.V. The influence of the conditions of hydrothermal synthesis on phase states and particle size of ZrO_2

key words: [*zirconium dioxide, particle size, nanocrystal, hydrothermal synthesis*]

Synthesis and investigation of zirconium dioxide with nanometric dimensions are of particular scientific interest for solving many questions of hydrothermal chemistry and mineralogy of nanocrystals. Moreover, producing ultradispersed powders on the base of zirconium dioxide has an important application for creating materials with high impact resistance, producing heat resistant elements and solid electrolytes for electrochemical power suppliers.

Zirconium oxyhydroxide was used as a starting material for hydrothermal synthesis. It was obtained by the following reaction:

$ZrOCl_2 + 2NH_4^+OH \rightarrow ZrO(OH)_2 + 2NH_4^+Cl$.

The reaction product was comprised of the polymer type hydroxycomplex in an X-ray amorphous state.

Zirconium oxyhydroxide dehydration was performed in hydrothermal conditions at temperatures 200-350° and pressures 30-90 MPa, synthesis duration was 1-24 h, and variable chemical nature of hydrothermal solutions (aqueous solutions of alkali metal halides).

The obtained powders were studied by the methods of X-ray phase analysis (XPA), differential thermal analysis (DTA), and electron microscopy.

The data of XPA and electron microdifraction analysis testified that only zirconium dioxide was in crystalline state after hydrothermal treatment .

Identification of particle distribution by size and determination of mean particle dimensions were conducted by analyzing data of electron microscopic studies, with the help of computer image analyzer ‘Videotest 2.0’, as well as widening of the lines of corresponding phases on X-ray patterns of the samples. The obtained data testify to rather specific performance of particle distribution by size. The value of shape factor showed that all particles may be referred as spheroidal with a high accuracy. The analysis of sample X-ray patterns and microphotos, obtained by electron microscopy, suggests only a weak correlation between zirconium dioxide phase state and mean size of the particles. It was also stated by some authors. An increase in temperature and synthesis time led to insignificant enlargement of dimensions of the particles that were both nonequilibrium at given temperatures (tetragonal and cubic [t+c] ZrO_2 modifications) and equilibrium (monoclinic modification).

The change of hydrothermal treatment conditions has a significant effect on the phase state of zirconium dioxide powders. For instance, an increase in treatment temperature from 250 to 350°C led to almost complete disappearance of [t+c] ZrO_2 modifications.

The variations of hydrothermal solution chemical compositions were also responsible for changing the phase state of ZrO_2 nanocrystals. The aqueous solutions of alkali metal halides were used in this work as the hydrothermal solutions. The data of X-ray analysis show that the highest yield of the total quantity of [t+c] modifications was achieved when using distilled water and LiCl solution as hydrothermal solution. Using alkali metal fluorides as hydrothermal solutions results in mainly the monoclinic modification of zirconium dioxide. This fact can be explained by isomorphism in cation and anion sublattices that was confirmed by the chemical analysis of the powders.

The zirconium dioxide powders of nanometric dimensions obtained by hydrothermal dehydration differ considerably in morphology and specific particle size distribution from nanometric powders obtained by other methods. However, the similarity of zirconium dioxide nanocrystal morphology with morphology of some types of silica nanominerals (opal and the like), also obtained in hydrothermal conditions, should be noted.

#Kovalskii A.M., Kotelnikov A.R., Chichagov A.V., and Suvorova V.A. Synthesis and refinement of unit-cell parameters of (K,Rb)-feldspars

key words: [feldspars, X-ray investigation, unit-cell parameters, ordering, disordering, albite, microcline, sanidine]

The synthesis of ordered and disordered $(K,Rb)AlSi_3O_8$ solid solutions was conducted by two techniques:

- ion exchange in salt melts in quartz containers;
- hydrothermal synthesis by the ampoule technique.

The X-ray investigation and refinement of unit-cell parameters (UCP) has been performed for all the synthesized samples. Samples were analyzed in the continuous scanning operation of full X-ray diffraction profile by automatic diffractometer PC/HZG-4. The angle positions were evaluated using Spectr-8 computer program (Okhulkov A.V., IEM RAS) with correction to the inner standard (Si of spectral purity, a=5.4305 Å). From 25 to 61 reflexes in the angle interval 7-39° (θ) were used to refine the unit-cell parameters. The refinement was made using computer programs LCC, PUDI [1,2].

Synthesis of (K,Rb)-feldspar solid solutions by the method of ion exchange in the salt melts and refinement of their UCP

Natural ‘low’ albite N4 (Vishnevye mountains, South Ural) was used as a starting material for the synthesis. The albite chemical composition (wt%) is: Na_2O – 12.03; Al_2O_3 – 19.07; SiO_2 – 68.70; K_2O – 0.15; CaO – 0.05. Recalculation to 8 atoms of oxygen gives the formula: $Na_{1.02}K_{0.01}Al_{0.98}Si_{3.00}O_8$.

The refinement of unit-cell parameters for this sample provided the following results:

a=8.1382(11) [Å]; b=12.7874(7) [Å]; c=7.1603(7) [Å]; α=94.277(6) [Å]; β=116.621(8) [Å]; γ=87.668(7) [°]; V=664.3(3) [Å^3].

‘High’ albite was obtained from ‘low’ Ab №4 through its disordering by the method of high temperature treatment at 1070°C during 61 days. The treatment was performed through the several stages. Control over the degree of ordering was carried out by the X-ray analysis. The parameters of fully disordering Ab N4 are as follows:

a=8.154(1) [Å]; b=12.874(1) [Å]; c=7.112(1) [Å]; α=93.39(1) [Å]; β=116.46(1) [Å]; γ=90.29(1) [°]; V=666.9(2) [Å^3].

For the purpose to obtain pure $KAlSi_3O_8$ (‘low’ and ‘high’), ion exchange (Na ↔ K) between KCl melt and two minerals (1) initial Ab N4 (‘low’) and (2) ‘high’ albite, obtained from Ab N4, was conducted. The runs were carried out in quartz containers with the ratio of Ab charge – KCl as 1:20. Containers were held at temperature

---

[#] This work was supported by a grant RFBR 97-05-65886.

850°C and atmospheric pressure during 10 days. As a result of the experiments, microcline and sanidine were obtained with the following unit-cell parameters:

microcline: a=8.591(1) [Å]; b=12.971(1) [Å]; c=7.221(1) [Å]; α=90.61(1) [Å]; β=115.94(1) [Å°]; γ=87.64(1) [Å]; V=723.0(2) [$Å^3$].

sanidine: a=8.605(1) [Å]; b=13.031(1) [Å]; c=7.182(1) [Å]; β=116.029(12) [°]; V=723.8(3) [$Å^3$].

Solid solutions of 'low' and 'high' $(K,Rb)AlSi_3O_8$ were synthesized by ion exchange (K ↔ Rb) of microcline and sanidine samples, respectively, with RbCl melt. The experiments were also performed in quartz containers with the ratio of $KAlSi_3O_8$ charge – RbCl melt as 1:20. Containers were held at temperature 850°C and atmospheric pressure during 13 days. Structural state of microcline during the experiment was controled by the method of parallel run with 'mineral-witness'. As a result of the experiments, solid solutions of ordered and disordered $(K,Rb)AlSi_3O_8$ with rubidium end member content of 95 mol% and 76 mol%, respectively, were obtained.

The refinement of unit-cell parameters for the members of 'low' and 'high' series yielded the following results:

microcline: a=8.841(1) [Å]; b=12.964(1) [Å]; c=7.254(1) [Å]; α=90.519(9) [Å]; β=116.190(6) [Å]; γ=88.004(8) [°]; V=745.64(15) [$Å^3$].

sanidine: a=8.843(2) [Å]; b=13.032(2) [Å]; c=7.200(2) [Å]; β=116.313(13) [Å]; V=743.76(34) [$Å^3$].

The obtained results on Rb-bearing analog of microcline are in a good agreement with data of McMillan et al. [3].

Hydrothermal synthesis of (K,Rb)-feldspar solid solutions and refinement of their UCP. Synthesis was conducted by the ampoule technique at temperature 650-700°C and P_{H2O}=1-5 kbars. The duration of runs was up to 24 days. Gel mixtures of (K,Rb)-feldspars were used as starting materials. The mixtures of potassium-rubidium feldspars and leucites were obtained as products of experiments at T=700°C and P_{H2O}=1 kbars, and $X_{Rb}>0.5$. Temperature decrease to 650°C and pressure increase to 5.3 kbars enhanced stability of feldspars in relation to leucite.

Solid solutions of (K,Rb)-feldspars were synthesized with X_{Rb}=0.0, 0.2, 0.3, 0.4, 0.5, 0.6, 0.8, 1.0 and their unit-cell parameters were refined. The dependence of unit-cell parameters on the composition of solid solution was close to linear. This dependence was approximated by the equation:

$$P = A + B * X_{Rb}^{Fsp} + C * (X_{Rb}^{Fsp})^2 + D * (X_{Rb}^{Fsp})^3;$$

where P is a unit-cell parameter.

The values of polynomial coefficients are presented in Table:

P	A	B	C	D	E*
a, [Å]	8.606611	0.2167950	0.0901870	-0.0716090	0.005
b, [Å]	13.031122	-0.0445400	0.1617590	-0.1115140	0.002
c, [Å]	7.149736	0.0076170	0.0395930	-0.0319670	0.002
β, [Å]	116.021677	0.2331520	0.1281280	-0.1049400	0.01
V, [$Å^3$]	723.5680	15.26733	19.45779	-14.64113	0.6

* approximation error

References:

1. Burnham C.W. IBM computer program for least-squares refinement of crystallographic lattice constants. Geophys. Lab. Carnegie Inst. Washington, D.C., Yearbook, 1962, v.61, p.132-135.
2. Burnham C.W. Least-squares refinement of crystallographic lattice parameters for IBM PC/XT/AT and compatibles, Harward University, Cambridge MA02138, 1991 (program description, 24 p.).
3. McMillan P.F., Brown W.L., Openshaw R.E. The unit-cell parameters of an ordered K-Rb alkali feldspar series. Amer. Miner., 1980, v.65, pp. 458-464.

Kotelnikov A.R., Kovalskii A.M., Suvorova V.A., Martynov K.V., Akhmedzhanova G.M., Gerasimova E.V., and Kurbyko T.A. Synthesis and investigation of properties of Ti-bearing minerals

key words:[*synthesis, perovskite, zirconolite, X-ray investigation, unit-cell parameters*]

Solid solutions of Ti-bearing minerals (perovskite and zirconolite) were synthesized by the methods of pyrosynthesis and hot isostatic pressing.

(Ca,Sr)-perovskite solid solutions were obtained by the pyrosynthesis. Mixtures of $CaCO_3$, $SrCO_3$, and TiO_2, taken in stoichiometric ratios, were used as starting materials. Thoroughly mixed, initial charges were pressed as tablets. Pressed tablets in alundum crucibles were loaded into high temperature furnace with chromite-lanthanum heater and held at 1375°C during 48 hours. The compositions of synthesized perovskites correspond to the stoichiometry of minerals in $(Ca,Sr)TiO_3$ series (Table 1). However, along with pure perovskites, the following phases were identified in the products of some experiments: rutile, Al-bearing perovskite, (Ca,Sr)O phase, $Ca_{6.2}Sr_{8.0}Al_{4.8}Si_{2.5}Ti_{2.4}O_{24}$ phase.

Table 1. The compositions and coefficients of crystallochemical formulas of (Ca,Sr)-perovskites obtained by the method of solid-phase synthesis (1375°C, the duration of experiments 48 hours).

N run	4901	4902	4903	4904	4905	4906

TiO_2,	59.08	55.30	52.02	51.27	48.77	45.47
CaO	40.93	32.09	28.79	22.10	16.64	9.04
SrO	-	12.61	17.74	26.42	34.17	44.69
Coefficients of crystallochemical formulas (recalculation to 3 oxygen atoms).						
Ti	1.00	1.00	0.97	0.99	0.98	0.97
Ca	1.00	0.83	0.77	0.61	0.48	0.27
Sr	0	0.18	0.26	0.39	0.53	0.74
$X_{Sr}^{P_{cr}*}$	0	0.18(5)	0.25(4)	0.39(4)	0.52(7)	0.73(12)

* - strontium mole fraction in solid solution.

The refinement of unit-cell parameters was performed for this series of solid solutions. Samples were examined in the continuous scanning operation of full X-ray diffraction profile by automatic diffractometer PC/HZG-4. The evaluation of reflex angle positions was performed by Spectr-8 computer program (Okhulkov A.V., IEM RAS) with correction to the inner standard (Si of spectral purity, a=5.4305 Å). From 4 to 15 reflexes in the angle interval 7-39° (θ) were used to refine the unit-cell parameters. The refinement was made using computer programs LCC, PUDI [1,2]. The calculated values of unit-cell parameters of (Ca,Sr)-perovskites are presented in Table 2. It must be noted that synthesized perovskites have a orthorombic syngony up to compositions with $X_{Sr}^{Per} = 0.18$ but a cubic syngony at $X_{Sr}^{Per} \geq 0.25$. The unit-cell parameters of (Ca,Sr)-perovskites with cubic syngony were described by linear expressions:

$a = 3.8395 + 0.06791 * X$ [Å] (±0.003);

$V = 56.587 + 3.0605 * X$ [Å] (±0.1).

Table 2. The unit-cell parameters of (Ca,Sr)-perovskite solid solutions.

N run	$X_{Sr}^{P_{cr}*}$	a,[Å]	b,[Å]	c,[Å]	v, [Å^3]	n**	syngony
4901	0.0	5.441(1)*	7.644(3)	5.380(1)	223.77(7)	15	orthorombi
4902	0.18	5.425(2)	7.701(8)	5.375(17)	224.57(74)	6	orthorombi
4903	0.25	3.856(1)	-	-	57.34(2)	4	cubic.
4904	0.39	3.868(1)	-	-	57.85(4)	4	cubic.
4905	0.52	3.871(1)	-	-	58.02(3)	4	cubic.
4906	0.73	3.893(1)	-	-	58.98(6)	4	cubic.
4907	1.0	3.906(1)	-	-	59.59(1)	5	cubic.

* - errors of UCP refinement are presented in parentheses and referred to the last tenth characters; ** - the number of reflexes used in UCP refinement.

Ca,Sr-zirconolites were synthesized by the method of hot pressing in three stages:

1) drying of starting materials in vacuum at 850°C during 0.5 hours;
2) pressing at 1350°C and end thrust 300 bars during 0.5 hours;
3) completion of the synthesis at 1350°C and residual end pressure (50) bars during 4 hours.

Synthesized zirconolite samples were characterized by the phase homogeneity but Zr/Ti ratio varies in a rather wide range. Perovskite and zirconolite stability to leaching processes studied by the test technique MCC-1 of International Atomic Energy Agency (IAEA). The rates of strontium and calcium leaching (duration of experiment 47 days) were 0.006–0.01 g/(m^2*day). It allows to use these minerals as matrixes for radionuclide immobilization.

Conclusion.

Binary solid solutions of (Ca,Sr)-perovskites are synthesized at temperature 1375°C.

The unit-cell parameters of (Ca,Sr)-perovskites are refined by X-ray diffraction method. It is shown that: (1) the series of perovskite solid solutions are characterized by rhombic syngony (up to $X_{Sr}^{Per} = 0.18$) and cubic syngony at $X_{Sr}^{Per} \geq 0.25$; (2) the unit-cell parameters of perovskites with cubic syngony are described by linear composition dependence.

(Ca,Sr)-zirconolites are synthesized by the method of hot isostatic pressing at 1350°C.

Testing under the MCC-1 technique reveals high stability of perovskites and zirconolites to the leaching processes.

References:

1. Burnham C.W. IBM computer program for least-squares refinement of crystallographic lattice constants. Geophys. Lab. Carnegie Inst. Washington, D.C., Yearbook, 1962, v.61, p.132-135.
2. Burnham C.W. Least-squares refinement of crystallographic lattice parameters for IBM PC/XT/AT and compatibles, Harward University, Cambridge MA02138, 1991 (program description, 24 p.).

Kotelnikov A.R., Kovalskii A.M., Karyaeva E.G., Orlova A.I., Petkov V.I., Akhmedzhanova G.M., and Ushakovskaya T.V. Investigation of (Na,Sr)-zirconium-phosphate solid solutions

key words: [*solid solutions, zirconium-phosphate, X-ray investigation, unit-cell parameters*]

The ceramic materials based on zirconium-phosphates (with general formula MeI,MeII(MeII,Zr)$_2$(PO$_4$)$_3$, where MeI – Na, K, Rb, Cs, Mg, Ca, Sr, Ba; MeII – La…Lu, U, Pu…Am) are promising matrixes for immobilization of radionuclides from radioactive wastes due to high stability to leaching processes [1]. Hereafter we shall use the term 'NZP phase' to mean zirconium-phosphates. In order to predict the behavior of NZP matrixes in Earth's crust, it is necessary to know their thermodynamic properties and mechanism of cation-exchange reactions with fluid. For this purpose, the ion-exchange experiments in the system NZP – fluid were performed in hydrothermal conditions. The data on unit-cell parameters (UCP) of NZP phases are presented in [2]. However, the dependence of parameters upon the composition of solid solutions of (Na,Sr)-bearing NZP phases is absent. We have conducted the X-ray investigation of NZP solid solutions to refine their UCP.

Technique of experiment. The experiments were carried out under the ampoule technique in the apparatus of high pressure with cold sealing and external heating. The accuracy of temperature regulation was ±5°C and pressure regulation ±50 bars. The duration of experiments was 15 days. Phase and chemical composition of experiment solid products were determined by X-ray and microprobe methods but solutions were analyzed by AAS (atomic absorption spectroscopy). (Na,Sr)-zirconium-phosphates were identified as a single phase in the solid products of experiments from the results of X-ray study.

Results of experiments. Sodium and strontium distribution was studied in the system fluid - (Na,Sr)-NZP. The experiments were performed at 700°C, P = 2 kbars in 1M solutions (NaCl + $SrCl_2$).

The ion-exchange reactions of the following type were investigated:

$$NaZr_2(PO_4)_3 + 0.5SrCl_{2(fl)} = Sr_{0.5}Zr_2(PO_4)_3 + NaCl_{(fl)} \qquad (1)$$

The distribution of sodium and strontium between NZP and fluid was imperfect. Strontium enriched the fluid in relation to NZP phase in the full composition range. NZP compositions in experiment products of single run varied in the range 1-4 mol%. It testifies about complete ion-exchange reaction proceeding and attainment of equilibrium in the system.

X-ray analysis of NZP solid solutions

The X-ray examination of NZP phases was performed in the continuous scanning operation of full X-ray diffraction profile by automatic diffractometer PC/HZG-4. The evaluation of reflex angle positions was performed by application of Spectr-8 computer program (Okhulkov A.V., IEM RAS) with adjustment to the inner standard (Si of spectral purity, a=5.4305 Å). From 10 to 28 reflexes in space group R3c in the angle interval 7-39° (θ) were used to refine the unit-cell parameters. The refinement was made using computer programs LCC, PUDI [1,2].

The values of unit-cell parameters of NZP solid solutions as a function of Sr mole fraction are presented in Table 1. UCP concentration dependence of (Na,Sr)-NZP was characterized by nonlinear curves. This dependence was approximated by polynomial expressions of third order:

$$a = 8.8022 + 0.05240 * X - 0.437312 * X^2 + 0.291358 * X^3 \; [\text{Å}] \; (\pm 0.003) \qquad (2)$$

$$c = 22.7822 + 0.16733 * X + 1.62439 * X^2 - 1.229803 * X^3 \; [\text{Å}] \; (\pm 0.02) \qquad (3)$$

$$V = 1528.6 + 30.312 * X - 46.49566 * X^2 + 20.88518 * X^3 \; [\text{Å}] \; (\pm 1.1) \qquad (4)$$

where X is the mole fraction of strontium in NZP solid solution.

Table 1. The unit-cell parameters of (Na,Sr)-zirconium-phosphate solid solutions.

N run	X_{Sr}^{NZP}	a[Å]	c[Å]	V, [Å^3]	n**
*	0.00	8.803(1)	22.764(3)	1527.8(2)	24
4823	0.04(2)	8.805(1)	22.803(3)	1531.0(2)	23
4824	0.11(3)	8.801(1)	22 ?,211'2)	1530.8(1)	24
4847	0.14(1)	8.802(1)	22.857(2)	1533.5(2)	28
4825	0.23(3)	8.792(1)	22.880(5)	1531.5(3)	22
4826	0.26(3)	8.792(1)	22.908(4)	1533.7(2)	26
4881	0.49(3)	8.758(1)	23.102(2)	1534.7(2)	21
4827	0.531-2)	8.752(1)	23.151(2)	1535.7(1)	30
4880	0.65(3)	8.734(1)	23.239(3)	1535.3(2)	24
3774»	0.76(3)	8.717(1)	23.292(4)	1532.8(2)	24
4X79	0.89(3)	8.702(1)	23.381(3)	1533.2(2)	24
*	1.00	8.712(2)	23.33(1(4)	1533.7(6)	10

* - samples synthesized by sol-gel technique; ** - errors of UCP refinement are presented in parentheses and referred to the last tenth characters; *** - the number of reflexes used in UCP refinement.

Conclusion

Solid solutions of (Na,Sr)-zirconium-phosphates were synthesized at temperature 700°C and pressure 2 kbars. It was demonstrated that (Na,Sr)-NZP form continuous solid solution at given conditions.

Sodium and strontium distribution was studied in the system (Na,Sr)-NZP – fluid. It was recognized that distribution of Na and Sr in this system is imperfect, strontium enriched fluid in relation to NZP in the full composition range.

The X-ray investigation was performed for the series of (Na,Sr)-zirconium-phosphate solid solutions. On the basis of this study, the refinement of unit-cell parameters was carried out. UCP concentration dependence of (Na,Sr)-zirconium-phosphates was calculated.

References:

1. Orlova A.I., Zyryanov V.N., Kotelnikov A.R., Demarin T.V., and Rakitina E.V. (1993) Ceramic phosphate matrixes for high level wastes. Behavior in hydrothermal conditions. // Radiochemistry , v.35, n.6, pp.120-126.
2. Petkov V.I., Orlova A.I., and Egorkova O.V. By the existence of phases with $NaZr_2(PO_4)_3$ structure in the series of double orthophosphates with various ratio of alkali element and zirconium. // Journal of Structural Chemistry, 1996, v.37, n.6, pp.1104-1113.
3. Burnham C.W. IBM computer program for least-squares refinement of crystallographic lattice constants. (1962) //Geophys. Lab. Carnegie Inst. Washington, D.C., Yearbook, v.61, p.132-135.
4. Burnham C.W. (1991) Least-squares refinement of crystallographic lattice parameters for IBM PC/XT/AT and compatibles, Harward University, Cambridge MA02138, (program description, 24 p.).

Terent'ev A.V., Kunts A.F. Solid-state recrystallization of mineral aggregates of carbonate rocks (experimental models)

key words [*calcite dolomite recrystallization*]

Recrystallization of mineral aggregates appears widely in nature. Adequate attention, however, was not paid to systematic study of this process. Experimental studies, especially at high temperatures and pressures, i.e. conditions close to the natural, are not numerous.

First, the dependence of a degree of coarsening of calcite and dolomite grains on annealing temperature was studied (Table 1).

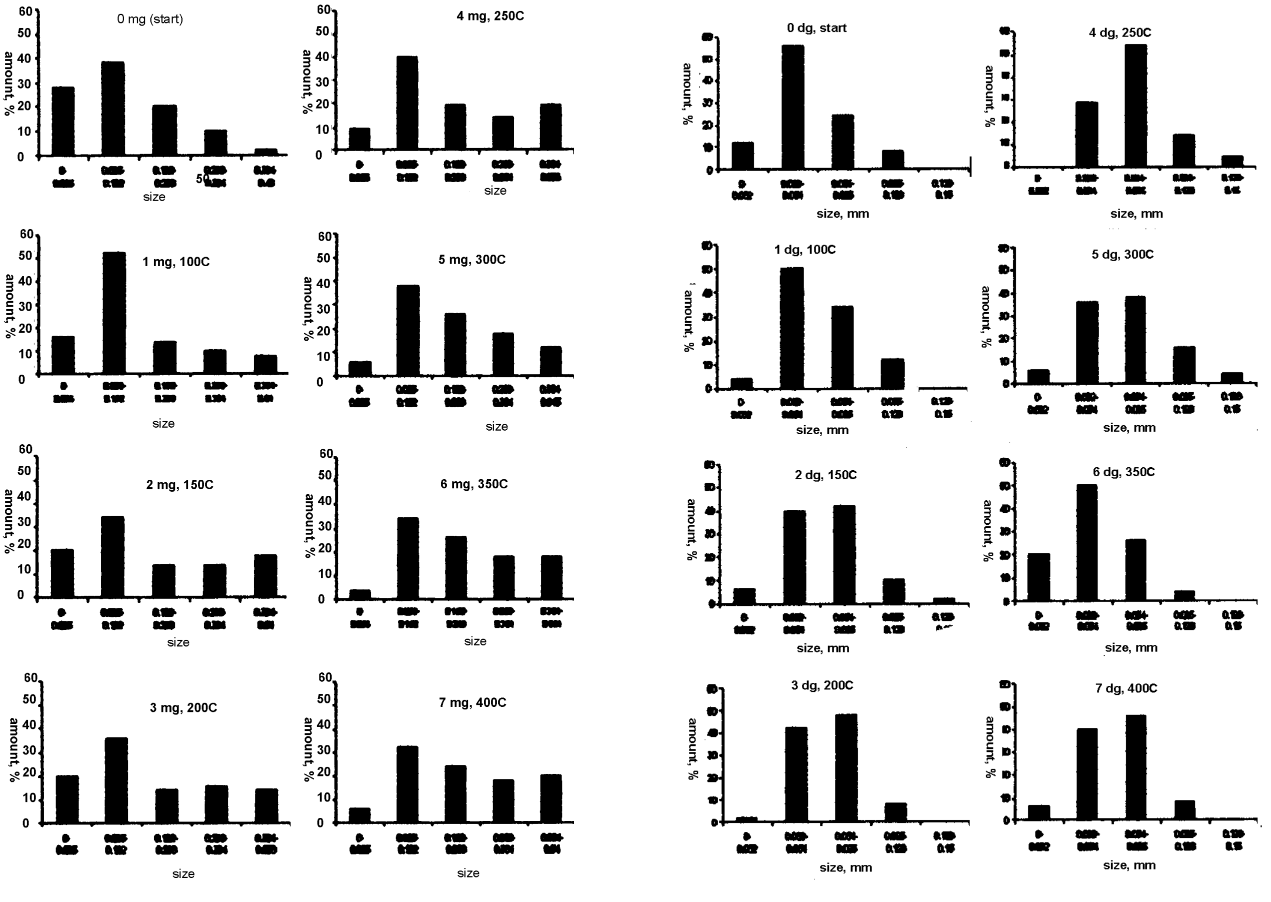

Fig.1. Change in grain sizes of a) calcite and b) dolomite aggregates depending on annealing temperature.

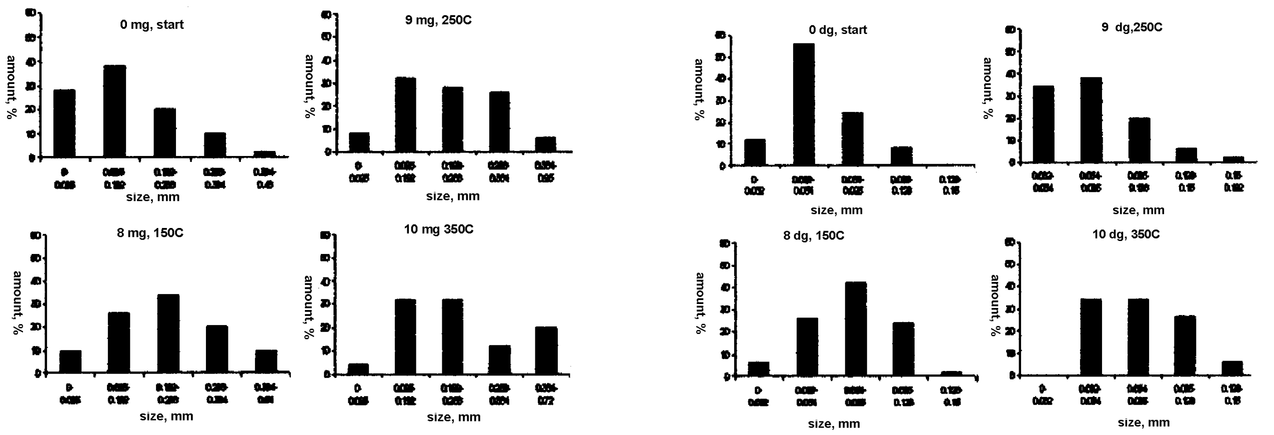

Fig.2. Change in grain sizes of a) calcite and b) dolomite aggregates depending on hydrothermal influence.

Table 1. Dependence of coarsening of calcite and dolomite grains on annealing temperature

Annealing temperature, ^{O}C	Mean size of calcite grains, mm	Coarsening of calcite grains, % of initial	Mean size of dolomite grains, mm	Coarsening of dolomite grains, % of initial.
-	0.178	-	0.066	-
100	0.198	11	0.073	11
150	0.231	30	0.074	12
200	0.234	31	0.076	15
250	0.257	44	0.086	30
300	0.272	53	0.080	21
350	0.264	48	0.063	-5
400	0.267	50	0.075	14

Table 2. Temperature dependence of coarsening of calcite and dolomite grains in hydrothermal conditions.

Temperature, ^{O}C	Mean size of calcite grains, mm	Coarsening of calcite grains, %	Mean size of dolomite grains,	Coarsening of dolomite grains, % of initial.
-	0.178	-	0.066	-
150	0.247	38	0.085	29
250	0.249	40	0.088	35
350	0.260	46	0.088	33

Some coarsening of a mean size of calcite grains in comparison with the initial is seen to be observed already at 100^{O}C. At 150^{O}C grain growth is more distinct and remains practically constant in the interval 100 - 200 ^{O}C. Maximum of coarsening occurs at 300^{O}C. The gradual growth of the mean grain size of dolomite grains is observed in the interval 100 - 200^{O}C. At 250^{O}C this value notably increases and corresponds to the maximal grain coarsening (30 % with respect of the initial). Grain sizes decrease with increasing temperature, and the process of recrystallization with decrease of grain sizes with respect to the initial is distinctly observed at 350^{o}C. The next grain coarsening takes place at temperature 400^{o}C.

After that, the processes of recrystallization were studied under hydrothermal conditions (Table 2). The major structural changes in marble and dolomite samples were observed at 150^{o}C. The changes are followed by monotonous increase in grain sizes with increasing temperature.

More representative picture of recrystallization in mineral aggregates is given in histograms of changing in sizes of calcite and dolomite grains (Figs. 1 and 2).

The histograms of distribution of grains by sizes in the calcite and dolomite aggregates show the regularities in grain coarsening, that previously had large sizes at the expense of dissolution of smaller grains. Increase of annealing temperatures and hydrothermal influence causes growth of larger grains. In fact, recrystallization of mineral aggregates in initial rocks is the major result of thermal influence in hydrothermal and metasomatic processes of mineral and ore formation.

Kim J.I., Burdina K.P., Zorov N.B., Kravchenko O.V., Kudryashov S.I., Kuzyakov Yu.Ya., Kulinich S.A. High-temperature and high-pressure treatment of amorphous carbon nitride with the β-C_3N_4 thin film as seed crystal

key words: [*carbon nitride pulsed laser ablation (PLA) direct current (DC) discharge, high-temperature and high-pressure treatment]*

Cohen and Liu (1989) theoretically predicted [1, 2], that crystalline β-C_3N_4 would have hardness comparable with diamond hardness. Later numerous experimental investigations on synthesis of crystalline β-C_3N_4 were carried out. The following reactions were used: a) plasmochemical reactions of methane with ammonia and nitrogen [3]; b) reaction of products forming at laser ablation of carbon-bearing materials with products of electric discharge in nitrogen [4]; c) reaction of products of cathodic sputtering of carbon in nitrogen atmosphere [5], etc. Forming carbon compounds were deposited as films on basement, made of material, whose crystallographic surface structure was similar to β-C_3N_4 structure. X-ray and electron diffraction studies showed, that the films contain the compound, which can be concerned to theoretically predicted β-C_3N_4. It is found, however, that depending on method of production the films contain 25-40 wt % of nitrogen, whereas β-C_3N_4 contains

57 wt % of nitrogen. It was proposed, that bulk composition of the films is conditioned by presence in them of diverse compounds of carbon with nitrogen, including β-C_3N_4. The purpose of the present study was a production of crystalline C_3N_4 in the conditions of high-temperature and high-pressure treatment of amorphous C_3N_4 using films, containing crystalline C_3N_4 as seed crystals.

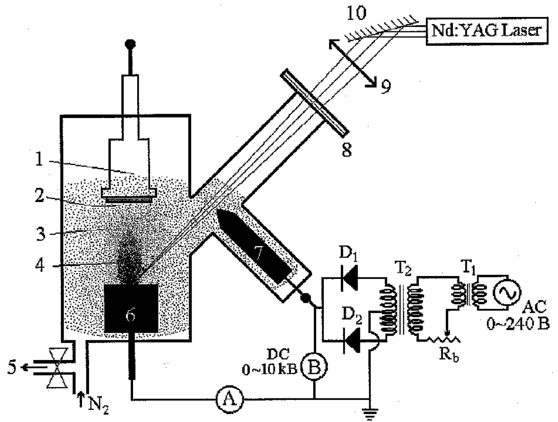

Fig. 1 Experimental assembly for deposition of the carbon nitride thin films. 1 - Holder; 2 - Si(100) basement; 3 - Discharge zone; 4 - Laser plume; 5 - to vacuum pump; 6 - Cathode; 7 - Anode; 8 - Glass window; 9 - Lense; 10 - Mirror

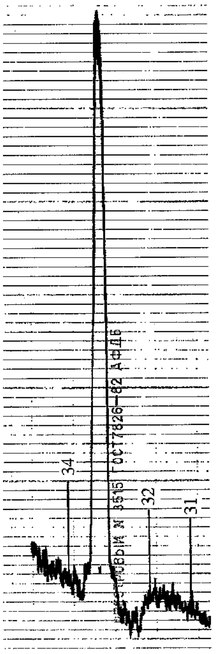

Fig. 2 X-ray diffraction (XRD) reflection of the β-C_3N_4 film.

In order to produce the films, the apparatus (Fig. 1) was constructed, that uses for synthesis of the compounds of carbon with nitrogen the reactions of products of glow discharge in nitrogen (at pressures 0.08 - 0.7 Torr) with atoms and clusters of carbon, produced at cathodic sputtering of a graphite target and simultaneous influence of laser irradiation causing appearance of torch. The second harmonic of Nd:YAG laser irradiation with fluence 15 J/cm^3 was used.

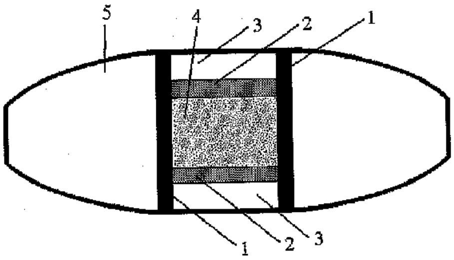

Fig. 3 Experimental assembly for high-temperature and high-pressure treatment. 1 - Heater; 2 - Si(100) basement with deposited C_3N_4; 3 - Thermal insulator; 4 - Amorphous C_3N_4; 5 - Container

The forming nitrogen compounds with carbon were deposited on a basement of monocrystalline Si(100), placed at distance of 20 mm over the cathode. In some experiments on plasma of glow discharge a magnetic field was imposed, that was created by electromagnet with flux density ~ 10 mT.

The produced films were studied by following methods. a) By infrared spectroscopy the peaks of C ≡ N, C = N, and C - N bonds in molecules were obtained. b) Auger spectroscopy showed, that spectrum contains C_{KLL} and N_{KLL} peaks. It was calculated from relation between intensity of these peaks accounting for sensitivity factors, that nitrogen content in the synthesized film is 25 %. c) Secondary ion mass-spectrometry (SIMS) showed the distribution of carbon and nitrogen atoms in the film. Using of cathodic sputtering without influence of laser irradiation on a target leads to formation of a film, which is half as thick. d) X-ray diffraction (Fig. 2) showed the peak $2\theta = 32.9^O$, that supports the presence in the film of monocrystalline compounds β-C_3N_4 of the β-Si_3N_4 structural type. e) Scanning electron microscopy showed, that sizes of seeds increase at imposition of a magnetic field. Magnetic field leads to formation of films, in X-ray spectra of which the intensity of the observed peaks increases.

The films, produced in the experiments upon laser irradiation and magnetic field, were used for high-temperature and high-pressure study. The films were used as seed crystals for crystallization of amorphous C_3N_4. The scheme of a sample preparation is shown in Fig. 3. The samples were studied in the pressure interval 10 - 70 kbar at temperatures 350 - 1200^{O}C. X-ray photoelectron spectroscopy showed, that the electron state of carbon nitride in the samples, treated at 70 kbar and 550^{O}C during 2 hours, differ from the electron state of carbon nitride in the amorphous sample. Authors suggest, that such changes are related to partial crystallization of amorphous C_3N_4.

References:

1. A. Y. Liu and M. L. Cohen, (1989) //Science 245, 841.
2. A. Y. Liu and M. L. Cohen (1990) //Phys. Rev. B 41 10727.
3. J. H. Kirn, Y. H. Kirn, D. J. Choi, H. K. Baik, (1996) // Thin Solid Films 289 79.
4. C. Niu, Y. Z. Lu and M. C. Lieber, (1993) // Science 261334.
5. D. G. McCulloch and A. R. Merchant, (1996) // Thin Solid Films 290/291 99.
6. P. W. Pahnberg, G. E. Riach, R. E. Weber, and N. C. MacDonald, (1972) //Handbook of Auger Electron

Spectroscopy (Physical Electronics Industries, Edina, Minnesota, 1972).

Redkin A.F., Ponomarev V.I., and Kostromin N.P. Hydrothermal synthesis and properties of sodium pentatungstate monohydrate $Na_2W_5O_{16}{\cdot}H_2O$

key words: [*hydrothermal synthesis, sodium polytungstates, unit-cell parameters, phase diagram*]

$Na_2W_5O_{16}{\cdot}H_2O$ was first obtained by hydrothermal synthesis from WO_3 in solution of 5-15 wt.% NaCl at 500°C, 400-500 bars as colorless mica-like crystals with specific weight 7.007±0.005 g/cm^3. It loses water in the range 440-660°C and transforms into $Na_2W_5O_{16}$ which incongruently melts at 770±5°C.

It was identified that $Na_2W_5O_{16}{\cdot}H_2O$ has a triclinic unit-cell with parameters:

a=17.91(1) Å, b=26.92(1) Å, c=39.93(1) Å, α=99.5(1)°, β=91.9(1)°, γ=98.6(1)°, V=18734 Å^3, and z=64. The X-ray pattern of the compound is presented in Table 1.

Phase diagram of sodium polytungstate stability in the right part of Na_2O-WO_3 system was refined. It is presented in Fig.1.

Table 1. The X-ray pattern of synthetic sodium polytungstate $Na_2W_5O_{16}{\cdot}H_2O$ (Na_2O-5.03±0.1, WO_3-93.67±0.1, H_2O-1.3 wt.%); CuK$_\alpha$, Ni-filter. Synthesis conditions: 500°C, 400 bars, starting solution of 15 wt.% NaCl, duration 14 days.

$d_{\alpha 1}$	I/Io	h	k	l	$d_{\alpha 1}$	I/Io	h	k	l
7.879	5	2	0	2	2.518	25	2	-9	-6
6.299	9	0	4	1	2.393	9	3	9	2
6.014	29	2	2	-4	2.353	7	3	8	6
5.887	21	3	0	0	2.062	7	1	-4	19
5.768	10	2	3	0	2.001	5	4	0	17
5.050	8	1	-4	-3	1.964	68	8	-7	-5
4.717	38	2	-4	-4	1.941	5	6	-6	-13
3.929	68	2	-5	7	1.841	6	8	-8	9
3.663	6	1	-4	-8	1.831	10	8	-9	-5
3.368	100	4	4	1	1.820	20	1	10	-18
3.157	93	0	8	-6	1.787	5	1	-10	-14
3.019	32	4	-6	7	1.736	6	6	10	-11
2.944	51	3	1	-12	1.703	5	4	-6	21
2.889	11	6	-2	3	1.602	15	5	-7	-19
2.673	6	6	-4	-5	1.581	12	5	1	-23
2.616	4	1	6	10	1.571	24	3	-1	24
2.583	5	3	1	-1					

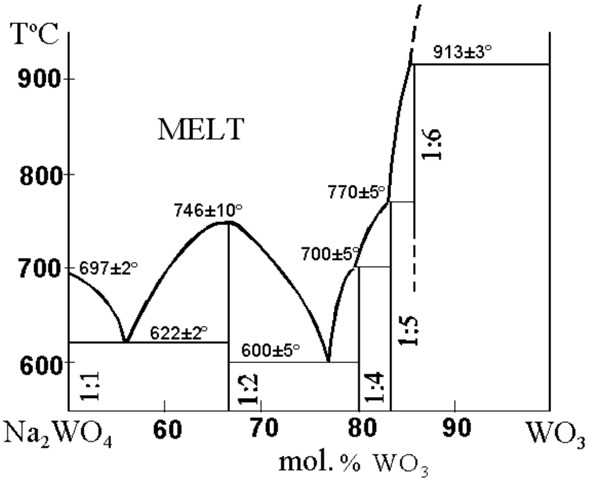

Fig.1. Prediction diagram of phase relations in the right part of Na_2O-WO_3 system.

Rusakov V.S., Kotel'nikova A.A., Lukanin O.A., Bykov V.N. Valence and structural state of iron atoms in basalt melts under pressures to 5 kbar.

key words[*iron basalt melt Mőssbauer spectroscopy*]

The effect of high hydrostatic pressure on the valence and structural state of iron atoms in natural basalt melts has been studied using the Mössbauer spectroscopy method.

The runs were conducted in a high pressure apparatus provided with an internal heating system at pressures to 5 kbar and constant temperature 1350^{o}C. The original basalt glass was enclosed in sealed platinum capsules of 5 mm in dia and 0.2 mm thick. The sample weight was 350-400 mg. A basalt glass powder was carefully dried and, right before welding the capsule, additionally annealed for 10 min at 700^{o}C. The pressure transmitting medium was argon. The exposure was from 11 min to 120 min. As suggested by the chemical analysis data, no change was found in the total iron content in the samples before and after the runs at various pressures and exposures which attested the absence of the interaction of the melt with the capsule walls.

The Mössbauer studies were performed at room temperature on a spectrometer of electrodynamic type, working in a constant accelerations mode. The spectra of the investigated samples were a superposition of two partial spectra of paramagnetic type, corresponding to Fe^{3+} and Fe^{2+} ions (Fig.1). In view of that, the processing and analysis of the spectra were conducted by restoring two independent distribution functions of the hyperfine interactions parameters of ^{57}Fe nuclei-shifts δ and quadrupole shifts ε.

Fig.2 illustrates the dependence of the intensity of the 1-st partial spectrum, corresponding to Fe^{3+} ions, on the applied pressure and the time-period of the attack. It can be seen that in the original glass the concentration of Fe3+ is $\approx$ 77%. As the sample is heated to 1350°C in a closed capsule, the concentration of Fe^{3+} ions increases by $\approx$ 10%. Under the action of the pressure iron experience partial reduction and, subsequently, the run duration (20 min) and temperature being invariant, its oxidation state remains practically constant. As the duration time increased to 120 min at 5 kbar, about 30% of Fe^{3+} ions is reduced to Fe^{2+}, the concentration of iron being invariant. Further reduction of iron ions was observed in the decompression run (fig.2) wherein the sample was subjected to a pressure of 5 kbar for 110 min with further 20 min exposure at a pressure of 0.16 kbar.

A FTIR-spectroscopy study of basalt glass samples has shown that they contain some water whose concentration depends on the run duration. In the samples obtained under high pressure with the exposure of 120-130 min the concentration of H_2O is much higher (0.5-0.7 wt%) than in the original glass and in the samples after the 11-20 min runs (0.05-0.1 wt%). So it is clear that the main cause of the partial reduction of ferric iron in the samples subjected to prolong pressure attack is hydrogen penetration out of the gas environment into the melt through the platinum capsule walls. In the gas environment a partial hydrogen pressure was generated due to the presence of water traces in the pressure transmitting gas medium (argon) and humidity of the heating system parts enclosed into the high pressure vessel.

An analysis of the distribution function parameters values of shifts δ and quadrupole shifts ε (fig.2) suggests the following conclusions. In 20 min runs no significant effect of pressure on the valence state of iron atoms in basalt melts is detected. The ferric iron in glasses being studied is in strongly distorted six-fold coordination, and ferrous iron is in tetrahedral coordination. The structural states of iron atoms are unaffected by the applied pressure and duration time. Irrespective of the pressure and run duration there are strong distortions of iron atoms environment polyhedra (for Fe^{3+} a range of variation of a mean distance to the nearest oxygen atoms is $\approx$0.05Å). As the run duration is increased at a pressure of 5 kbar, mean distances from iron atoms to the first coordination sphere increase (for Fe^{3+} by $\approx$0.03Å).

Note, that reduction of iron atoms in the studied glasses at an increased exposure time and a pressure change alike (see fig.2) leads to an increase of a mean distance to the nearest coordination sphere. With iron playing the part of cation-lattice former in these compounds, this is likely associated with the difference in ionic radii of Fe^{2+} and Fe^{3+}.

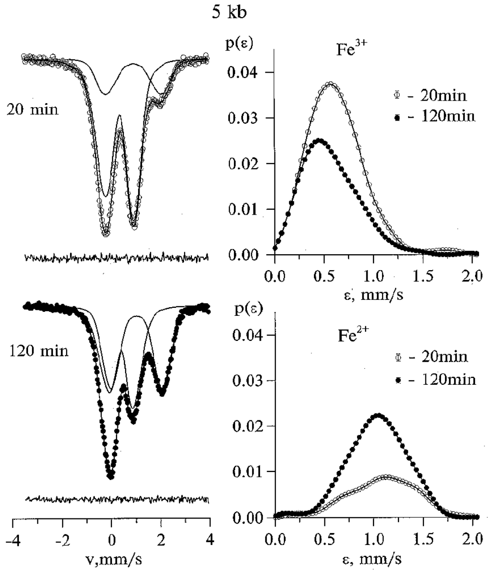

Fig.1. Characteristic Mössbauer spectra of the investigated samples and the results of restoration of the distribution function p(ε) of quadrupole shifts ε for Fe^{3+} and Fe^{2+} ions.

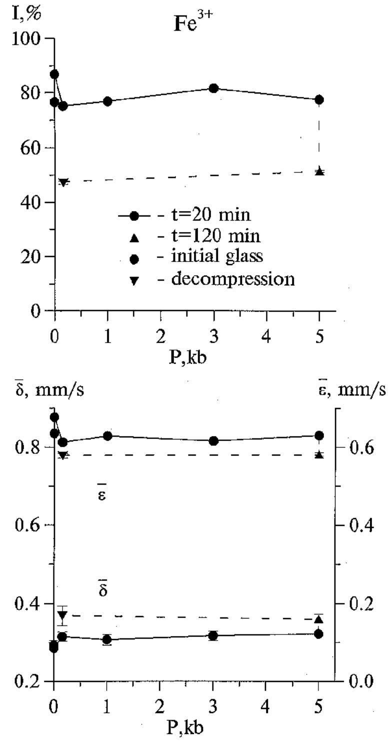

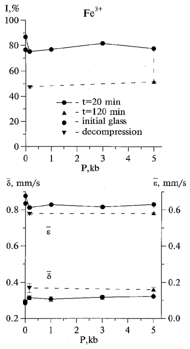

Fig.2. Dependences of the intensity of the 1-st partial; spectrum, corresponding to Fe^{3+} ions, Mössbauer line shifts δ and quadrupole shifts ε of this spectrum components on the applied pressure and exposure time period.

Kotelnikov A.R., Bychkov A.M., Akhmedzhanova G.M., Suvorova V.A., Gavlina O.T., Petukhov P.A., and Kovalskii A.M. Ecologically safe method for radioactive wastes disposal.

key words: [*radioactive wastes, sorption, phase transformation, mineral solid solutions*]

Purpose. At present, radioactive wastes in Russia and over the world are stored either as liquids in sedimentation tanks or as bound up elements in boron-silicate or alumino-phosphate glasses. The vitrification method, relatively cheap on the first stage of waste insulation, demands additional expenses in further: glasses must be held in a special storage since they have a relatively low stability upon aqueous solution influence and can not provide reliable and safe fixation for most radionuclides.

We have proposed the method of radioactive wastes binding into minerals (mineral matrixes) that are stable in the conditions of long storage in the Earth's crust.

The main conception of the method. A fundamentally new conception of radioactive wastes disposal has been proposed – conception of phase and chemical correspondence of matrix to wall-rocks of the Earth's crust. Two main aspects are used as a basis of conception:

1 – Dangerous materials should be disposal as compounds maximally close to natural, that have already showed their compatibility with biosphere during a long time (millions of years). Such compounds are minerals.

2 – minerals, containing radioactive wastes, must be in equilibrium with host rocks.

The description of process scheme. On the first stage, radionuclides are concentrated on zeolite sorbents (mineral-I ⇒ mineral-II on the scheme of Fig.1). On the second stage, zeolites are transformed into feldspars (mineral-III on the scheme) that are stable minerals widespread in nature. The described process is developed out for immobilization of strontium, cesium and iodine radionuclides. The investigations of obtained mineral matrixes by the test technique MCC-1 of International Atomic Energy Agency (IAEA) have shown their higher stability (by 2-3 orders) in relation to present-used matrix materials (Fig.2).

Phases	Mineral-I (zeolite ‘NaX’)	Mineral-II (zeolite ‘SrX’)	Mineral-III (Sr-feldspar)

Chemical reaction	Mineral-I ‘NaX’ + Sr^{2+} solution	Mineral-II ‘SrX’ - H_2O	Mineral-II⇒ Mineral-III
Process operation	Sorption ⇒ 25°C, flow	Dehydration ⇒ 400°C, atmosphere	Structural transformation 1000°C, annealing

Fig.1. Principal scheme of the process.

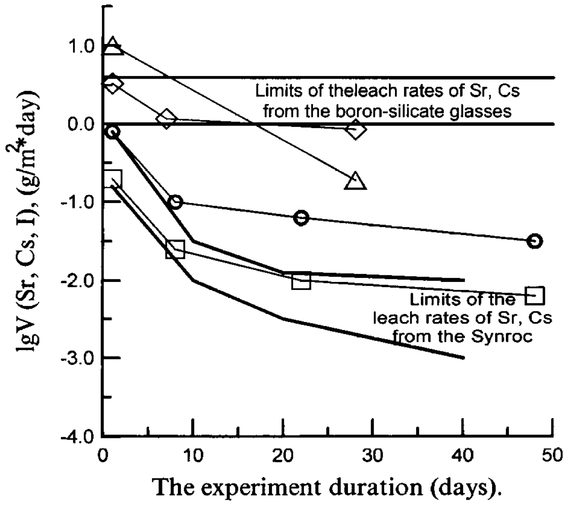

Fig.2. Logarithm values of leaching rates for strontium, cesium and iodine from various matrix materials versus duration of testing by IAEA technique. —(N,Sr)-feldspar, synthesized from zeolite; ϴ Cs-calcilith, synthesized from zeolite ; △ -bearing ceramics on the basis of zeolite ‘NaX’; ◊ I-bearing ceramics on the basis of zeolite ‘CuX’

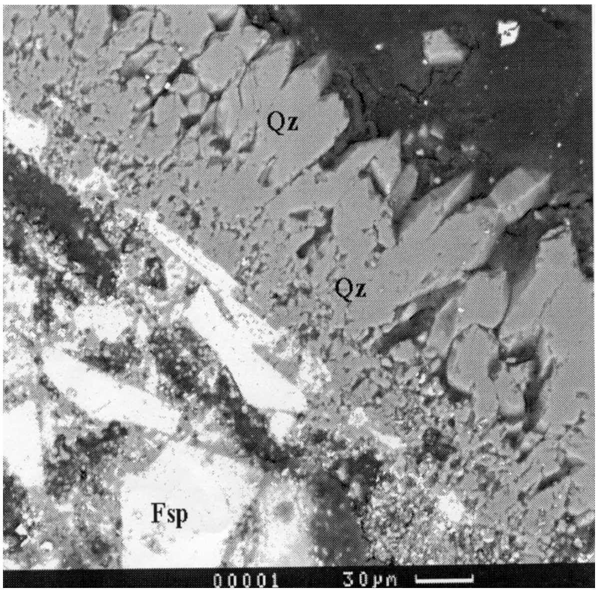

Fig.3. Double-layer matrix. Inner zone consists of (Na,Sr)-feldspar matrix (Fsp), outer zone – of quartz (Qz).

The promising direction of our study is a creation of ‘double-layer’ matrixes, based on phase correspondence of minerals having different composition. The principal scheme of the ‘double-layer’ matrix materials on the basis of coexisting minerals in the system $(K,Cs)AlSiO_4$ is shown in the Fig.3. The synthetic ‘double-layer’ matrix on the basis of (NaSr)-feldspars is also presented on Fig.3.

The advantages of the method

- possibility to process the solutions of radioactive elements having different concentration and composition;
- possibility of continuous control of the sorbent saturation process with radioactive elements;
- considerably higher stability (safety) of our matrixes in relation to all now-using matrix materials;
- sorption on the minerals from zeolite group is well technologically developed and extensively used for purification of various liquid wastes;
- relatively simple technological scheme of matrix production;
- preparation easiness of starting materials (natural and synthetic minerals from zeolite group) to use them as sorbents;
- low price for natural and synthetic minerals of zeolite group (possibility to apply already used in industry zeolites).